12-2018

Transient Absorption Microscopy, Instrumentation and Application to Amphotericin B

Kevin Higgins
University of Tennessee, khiggin8@vols.utk.edu

To the Graduate Council:

I am submitting herewith a thesis written by Kevin Higgins entitled "Transient Absorption Microscopy, Instrumentation and Application to Amphotericin B." I have examined the final electronic copy of this thesis for form and content and recommend that it be accepted in partial fulfillment of the requirements for the degree of Master of Science, with a major in Chemistry.

Tessa Calhoun, Major Professor

We have read this thesis and recommend its acceptance:

Michael Best, Frank Vogt

Accepted for the Council:
Dixie L. Thompson

Vice Provost and Dean of the Graduate School

(Original signatures are on file with official student records.)

Transient Absorption Microscopy, Instrumentation and Application to Amphotericin B

A Thesis Presented for the

Master of Science

Degree

The University of Tennessee, Knoxville

Kevin Higgins

December 2018

To my wife, Kali, without her love and support none of this would be possible.

Also to my girls, Makenzie and Madilynn.

Lastly to mom and dad.

Acknowledgments

This thesis would not have been possible without the love and support of so many individuals over the years.

First, I would like to thank my thesis advisor Dr. Tessa Calhoun who has been helpful and supportive throughout my graduate career. She has been patient when necessary and also tough when needed. I cannot thank her enough for the time and effort put in to making me into the chemist I am today. I would also like to thank my committee, Dr. Vogt, Dr Best, and Dr. Morrell-Falvey.

I would also like to thank all of the past and present Calhoun lab group members throughout the years for keeping me sane and making the work days bearable. Tyler, Phil, Breanna, Lindsey, Brandon C., Brandon W., and Redwan, you have each been helpful and motivational in your own ways.

I have to thank my family, and friends that have turned into family during my time at UT. My parents, who have been nothing but supportive throughout my whole process, and have provided stability when our family needed it. Maddi and William, while we haven't had the longest time together the two of you have helped me and my family survive our final years here and made them the best ones.

Lastly, I have to thank my wife, Kali. Whom graduate school has been most difficult on, but who has also been the most supportive and caring wife throughout the entire process. She has also given me my two greatest accomplishments during graduate school; my beautiful daughters Kenzie and Madi. It was a tough road but worth it in the end, thank you!

Abstract

Transient absorption microscopy (TAM) has emerged as a highly useful tool for studying a wide range of applications ranging from materials to biology. It has the advantage of being able to stimulate signal from non-fluorescent molecules and through microscopy is able to image these molecules without reliance on fluorescent quantum yield. A transient absorption microscope has been fully constructed and an initial instrumentation study is presented with white light compression and imaging of polystyrene beads in a solution of IR 1-44 laser dye. We are utilizing TAM for the study of the small-molecule antifungal, Amphotericin B (AmB) and how it interacts with living cells. There have been multiple studies conducted which present conflicting reports of the mechanism of action in which AmB is killing fungus. By directly imaging the AmB molecules interacting with the cells, we will be able to more clearly determine which, if any, of the previously proposed mechanisms is accurate. We have been able to image what we believe is AmB being internalized into yeast cells which is contradictory to the previously proposed mechanisms. While we have obtained preliminary images of the drug interacting with living cells, further investigations are necessary to obtain a full picture of the interactions with AmB and fungal cells.

Table of Contents

List of Figures

Chapter 1

Introduction

1.1 Motivation

There are approximately 11.5 million people each year that are affected by life-threatening fungal infections and over 1.5 million of those result in death.[9] A highly effective and standard of fungal treatment, Amphotericin B (AmB), has been in clinical use for over 50 years now and was placed on the World Health Organization's list of essential medicines in 2013. It has been placed on this list partly due to its high effectiveness over a wide range of fungal species, and partially due to limited occurrences of resistance seen over 50 years of continued use. The continued use with little known resistance is uncommon among many other anti-fungal drugs [62, 51]. While AmB is effective at disrupting membranes of fungal cells, it also comes with a list of potentially deadly side-effects for the patient. These can be less serious effects such as fever and chills to very serious side-effects including nephrotoxicity.[36, 47] As high as 25% of patients administered AmB will result in renal failure and/or death.[4] Determination of the MOA and the cellular targets of AmB, membrane-bound or internal, would be highly beneficial to the continuation of the pharmaceutical development. For example, the development of new drugs could be largely based on AmB with design alterations in order to reduce toxicity while retaining its effectiveness against infectious fungal cells. Multiple studies have been done in order to determine a mechanism of action (MOA) for AmB with conflicting results and proposed mechanisms. These mechanisms will be discussed in detail in Chapter 4. It has been proposed

that AmB targets the membrane of fungal cells and has a high affinity for cholesterol and its fungal derivative, ergosterol. Studies have shown that sterol contents in model membranes are possibly affecting AmB activity [52, 7], while similar studies on yeast cells have yielded inconsistent results.[69, 26] AmB has a very low fluorescent quantum yield (ϕ= 0.0006) making it impossible to directly image to learn where the molecule is entering the cells or how it is interacting with the membrane. This is an issue with many previous studies attempting to learn about the MOA of AmB. We plan to utilize the non-linear spectroscopy technique, transient absorption microscopy (TAM) in order to directly image AmB molecules interacting with fungal cells without the addition of labels or alterations of the drug in any way.

1.2 Non-linear Processes

There are multiple non-linear processes which we have utilized. The non-linear processes used include, two-photon fluorescence (TPF), second harmonic generation (SHG), and transient absorption (TA). As seen in Fig. 1.1 each of these non-linear processes utilize multiple light-matter interactions in order to produce the desired signal. With TPF, two photons of either the same or different energies are absorbed by the molecule to promote it to an excited state, where there is some loss of energy by non-radiative pathways, followed by a return to the ground energy state by way of fluorescence. This is also a spontaneous process, where the fluorescence is emitted in a non-coherent manner (in all directions). SHG converts two photons of identical energy to one photon with twice the energy instantaneously. SHG is only theoretically allowed from aligned, non-centrosymmetric molecules, meaning that they do not contain an inversion symmetry. This is often found at surfaces, interfaces or in specifically designed crystals to be used for SHG such as β-barium borate. SHG is also different from TPF in that it is a stimulated process, meaning that the emitted photons travel in a coherent manner and a specific direction.

Transient absorption is a non-linear absorption process that utilizes two ultrafast light pulses separated by a time delay, $\Delta\,\tau$, in order to probe the electronic structure of molecules and how they change with environmental variations. Transient signals can arise from multiple

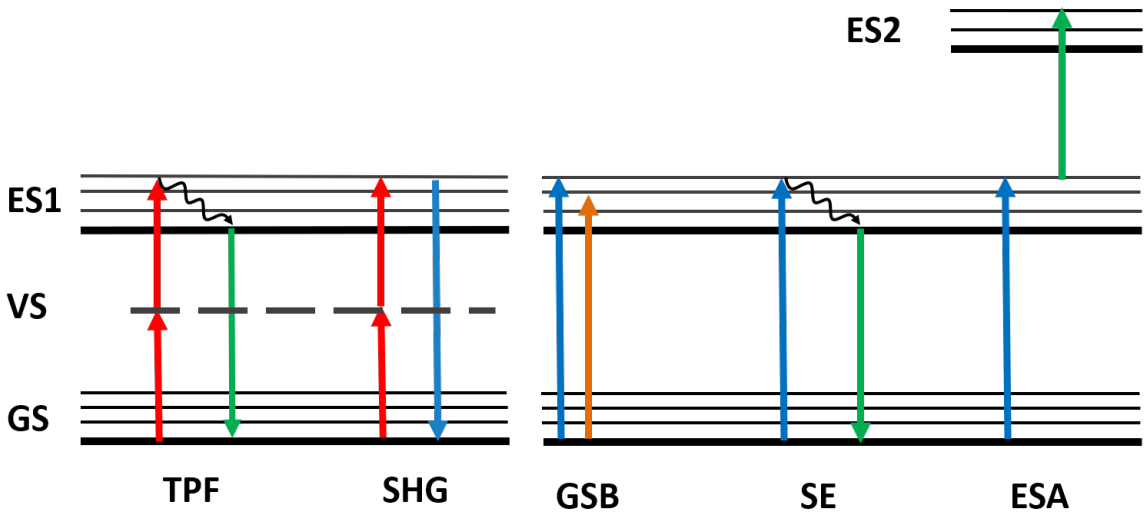

Figure 1.1: Energy level diagram depicting; two-photon fluorescence (TPF), and second harmonic generation (SHG). The three signals on the right side are possible sources of TA signal; ground state bleach (GSB), stimulated emmission (SE), and excited state absorption (ESA). GS - ground state, VS - virtual state, ES - excited state

sources dependent on the structure of the excited states, the energies used to probe the states, and $\Delta\,\tau$. This is depicted in Fig. 1.1, where three prominent TA signals are shown. Ground state bleach (GSB) signal arises from an initial pump pulse promoting electrons to an excited state, followed by a second pulse, probe, exciting remaining electrons from the ground state to an excited state.[13] Stimulated emission (SE) is generated from the same initial pump pulse being absorbed to an excited state where the probe pulse then arrives to stimulate emission from an excited state back to the ground state energy.[49] Finally, excited state absorption (ESA) arises from the initial absorption of the pump pulse to an excited state where the probe pulse arrives and is also absorbed from one excited state (ES1) to a second excited state (ES2). [24] In many cases for detection, the intensity at the wavelength of the probe pulse is monitored on a photon detector and small differences are detected in absorption or emission with the help of a lock-in amplifier. All of the above mentioned non-linear processes require a high density of photons on the sample in order for the low probability, multi-photon processes to happen. This can often be achieved by focusing a pulsed laser to a small point on the sample. This is attained for spectroscopy with the use of lenses which focus the light onto solutions.

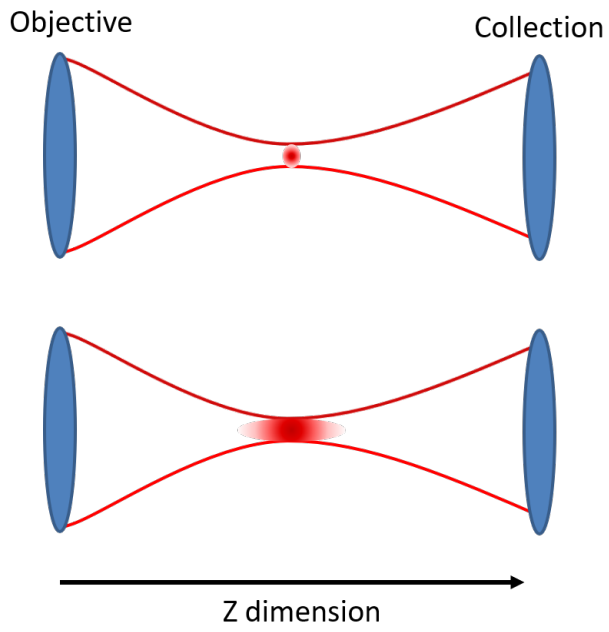

Figure 1.2: Illustration showing the difference between linear and non-linear microscopy. (Top) Signal from non-linear microscopy will arise from only the focal volume of the laser, (Bottom) signal in linear microscopy arising also from out of focus photons.

Non-linear microscopy utilizes microscope objectives for tight focusing of the light onto a sample of interest. Non-linear microscopy was first developed by Winfried Denk and James Strickler in the lab of Watt W. Webb at Cornell University in 1990. They took the previously developed idea of two-photon absorption and added a laser scanning component in a microscope to develop 'two-photon laser scanning fluorescent microscopy'. [18, 19] It has been shown that being able to excite chromophores in biological tissues and cells with lower energy light has lowered risks of tissue damage. These longer wavelengths are also scattered less when compared to the shorter wavelengths, which helps with improved signal to noise for higher resolution imaging. As a result of the necessary high density of photons for the non-linear processes to occur, all of the above mentioned processes also inherently have 3-dimensional optical sectioning capabilities. This means that the resulting non-linear signal will only arise from the focal spot of the laser and all out of focus light will not result in a noisy background signal, such as is the case in one-photon fluorescence. This concept is illustrated in Fig. 1.2. This is highly useful for non-linear imaging techniques for the acquisition of 3-D images. Transient absorption microscopy was developed later when

the first reports of pump-probe imaging with high repetition rate modulation schemes came from the Warren group where they measured ESA[24] studying melanin in B16 cells. Since then, TAM has been applied to study a variety of samples ranging from historical artwork [68] to energy flow in solar materials [29, 60]. We are applying the capabilities of TAM to biological samples and the study of the small molecule drug, AmB and how it is interacting with living fungal cells.

1.2.1 Overview

The initial steps of my thesis work were to construct and characterize an ultrafast transient absorption microscope. The construction design of the TA microscope has came from a previously built instrument in the Calhoun lab, with some significant changes. Full details on the instrumentation and design are discussed later in Chapter 2. Once the microscope was constructed, an initial instrumentation characterization study was completed through pulse characterization methods and the imaging of polystyrene beads, which is discussed in detail in Chapter 3. Finally, the TA microscope has been used to study the anti-fungal, AmB, and how it natively interacts with live fungal cells. For our studies we used *Saccharomyces cerevisiae* as our model fungal cell and the resulting images are shown and discussed in Chapter 4.

Chapter 2

Instrumentation

2.1 Introduction

Ultrafast transient absorption (TA) spectroscopy and microscopy are powerful tools for investigating photochemical and photophysical phenomena happening in the picosecond (ps) (10^{-12} s) and femtosecond (fs) (10^{-15} s) range.[20, 56] These measurements require two ultrafast laser pulses, known as a pump and probe pulse. An ultrafast laser is generally defined as a laser which produces pulses in the range of 100s of ps to single fs. For TA microscopy we obtain the ultrafast laser pulses from the output of a Ti:Sapphire oscillator. This is a high repetition rate (80 MHz) pulsed laser with relatively lower pulse energies, when compared to those often utilized in TA spectroscopy with amplified systems and kHz repetition rates. The repetition rate of a pulsed laser refers to the rate at which pulses are being emitted from the laser cavity. All lasers utilize an initial input energy and convert it into light through stimulated emission. Simple lasers are monochromatic, meaning that they are emitting light at a single wavelength. They also emit this light in a continuous, non-pulsing, mode. This is largely controlled by the choice of the lasing medium. Pulsed lasers are possible when the lasing medium has a large number of excited states at different energies as seen in Fig. 2.1. The different excited states are able to emit light at different wavelengths simultaneously. When a high number of excited states are emitting light, this leads to constructive and destructive interference from the wavelengths. When a large number of wavelengths have a constructive interference, this is known as 'mode-locked' and is controlled

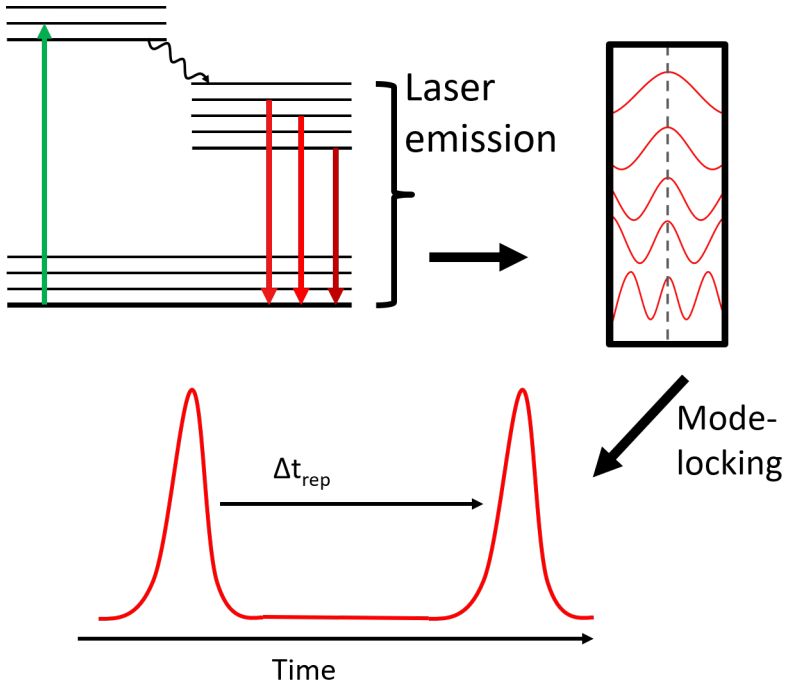

Figure 2.1: Illustration showing the multiple energy levels emitting light at different wavelengths, and how the mode-locking is achieved with the constructive interference of many wavelengths.

in our system with an acousto-optic modulator. With the introduction of a higher number of wavelengths being emitted from the lasing medium, a shorter laser pulse is possible, due to the narrower width of the overall constructive interference pattern. For the TA studies discussed here a Ti:Sapphire oscillator (MaiTai SpectraPhysics) was utilized with a center wavelength output of 800 nm, 12 nm bandwidth, an 80 fs pulse width, and 80 MHz repetition rate.

The experimental layout of the TA microscope that has been constructed using the Ti:Sapphire oscillator is shown in Fig.2.2. The individual components will be discussed in the following sections. From the output of the Ti:Sapphire oscillator the beam initially passes through a Faraday isolator to ensure that no reflections travel back into the laser cavity and disrupt mode-locking. This is followed by a waveplate and a polarizer beam-splitting cube in order to separate the beam into a pump and probe beams. The pump beam is sent through an electro-optic modulator for modulation of the repetition rate frequency, followed by the first prism compression line (see section **2.2.3**). The beam is then focused onto a β-Barium

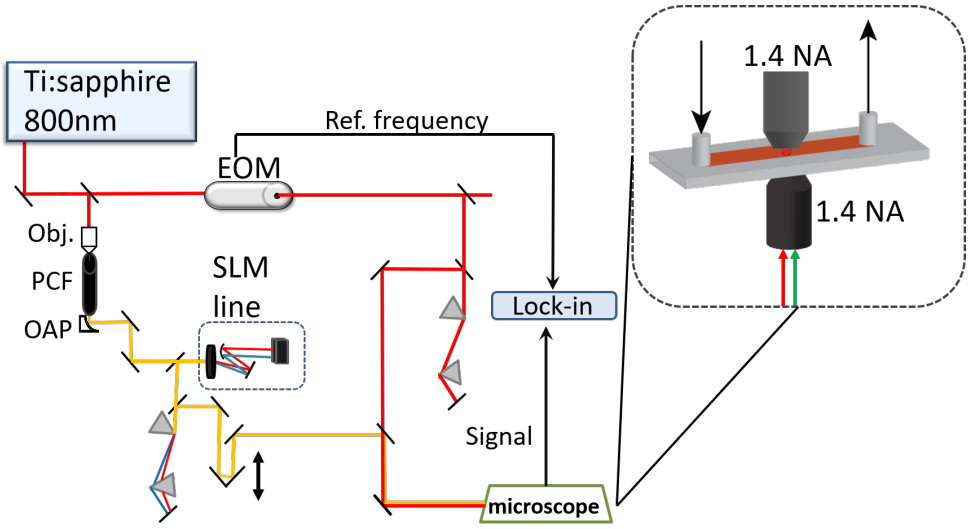

Figure 2.2: Experimental design of our TA microscope. The output of a Ti:Sapphire oscillator is split into a pump and probe beam. The pump beam is directed through an Electro-optic modulator (EOM) and a prism line for pulse compression before being sent into the microscope. The probe line is focused into a photonic-crystal fiber (PCF) with a 40X microscope objective (obj.) and collimated with an off-axis parabolic (OAP) mirror. The white light is compressed with a combination of SLM-based pulse shaper and a prism line (PL) before being combined with the pump beam and directed into the microscope. Top right inset shows the sample position with a 1.4 NA focusing and collection objective and the sample flowing through a homebuilt flow cell.

Borate (BBO) crystal for second-harmonic generation (SHG) of the 800 nm for conversion to 400 nm. As discussed previously, SHG takes two-photons of identical frequency and converts them to one photon at double the initial frequency. This beam is then sent through a second prism compression line before being directed into the microscope. The probe line is first focused onto a photonic-crystal fiber (PCF) for white light generation followed by a spatial-light modulator (SLM) based pulse shaping line followed by a prism compression line. The pump and probe beams are combined with a dichroic mirror, which passes the white light and reflects the pump laser, and reflected into the microscope co-linearly. Both beams are then focused onto the sample position with a 1.4 numerical aperture (NA) objective and the signal is collected with a second high NA objective before being directed to the desired detector.

2.2 Pulse Compression

Pulsed lasers emit light in a non-continuous mode, at a specific repetition rate (ranging from kHz to THz regime) with a wide range of pulse widths. Pulse widths are generally measured at the full-width half-maximum position of a Gaussian-like pulse. Pulsed lasers are now very common and are commercially available down to low femtosecond pulse widths. The bandwidth of our laser output is 12 nm FWHM which theoretically limits our pulse width to 78.5 fs. This is denoted as the Fourier-transform (FT) limited pulse width given by eq. 2.1. Where Δt is the FT limited pulse width, c_B is a time-bandwidth product (0.441 for a Gaussian pulse), λ is the center wavelength, $\Delta\ \lambda$ is the bandwidth, and c is the speed of light.

$$\Delta t = \frac{c_B \lambda^2}{c \Delta \lambda} \tag{2.1}$$

As seen from the equation the bandwidth of the laser pulse is inversely proportional to the pulse width, meaning that a larger bandwidth can result in a shorter pulse width. Pulses can become uncompressed for many reasons, the most prominent being travelling through different materials (lenses, polarizers, waveplates) where the change in refractive index alters the compression. Dispersion is introduced to the laser pulse when traveling through materials and lower energy wavelengths will travel at different speeds than higher energy wavelengths thus separating these wavelengths in time. This can be compensated for through different methods, and our implementation of two methods; prism-compression and pulse shaping, will be described below.

2.2.1 Pulse Characterization

Due to the ultrashort pulses in our laser system being in the femtosecond regime, electronics are not fast enough to resolve the pulse width. This leads to the need for other measures to be taken in order to accurately characterize the pulse width of our laser. We utilize a method known as autocorrelation, which uses one pulse of light to measure a second pulse of light. A diagram of an autocorrelator is shown in Fig. 2.3 where an input beam is first sent through a 50:50 beam-splitter and one arm is reflected to a retro-reflector which reflects

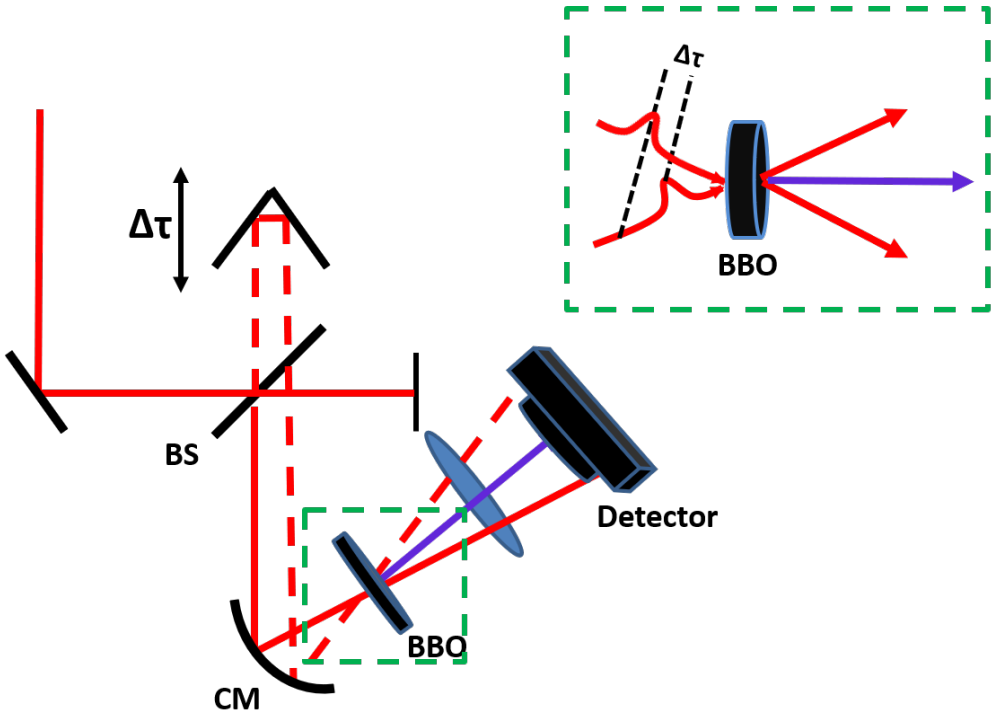

Figure 2.3: Schematic of an autocorrelator with the input beam passing through a beam-splitter (BS) where one arm (dotted line) is sent to a retro-reflector on a controllable stage and the other arm (solid line) is reflected back by a silver mirror. Both beams are then focused using a curved mirror (CM) onto a BBO crystal for SHG generation and focused onto a detector.

and translates the light vertically and horizontally from the input beam. This offset beam is known as the movable arm, due to the motorized stage that the retro-reflector is on. The arm that passes through the beam-splitter is reflected by a mirror directly back onto itself, and is known as the fixed arm. Both the movable and fixed arms of the autocorrelator are now sent back through the beam-splitter and directed onto a curved mirror. This mirror focuses both beams onto a BBO crystal for SHG generation. When both pulses of light are perfectly overlapped in time and space on the BBO crystal an SHG signal will be created utilizing one photon from each pulse creating a third beam of light located directly in the middle of the two input beams. This beam is focused onto and detected by a photodiode which is read out on the computer. The third beam of light is only possible for the duration that the two pulses are overlapped, so as the movable arm is scanned in space, we can monitor the SHG

signal for temporal duration and obtain an accurate measurement of the pulse width. This is done by relating the distance traveled of the movable stage to time with the speed of light.

2.2.2 Frequency Resolved Optical Gating

Autocorrelation measurements, using a photodiode for signal detection and pulse width measurements are highly useful and straightforward to achieve, but obtain no information about the phase or bandwidth aspects of the pulse. This is where another technique for pulse measurement becomes useful, known as frequency resolved optical gating (FROG).[64, 65] One FROG technique is able to utilize the same experimental setup as the autocorrelator, with the exception of the detector. Instead of focusing the SHG signal onto a photodiode, the light is sent into a spectrometer. For our system, we utilize USB spectrophotometers from OceanOptics allowing frequency bandwidth information and pulse width information to be acquired simultaneously. For the initial 800 nm pulse width measurements we used a technique known as SHG-FROG, an example measurement from our instrument of an SHG-FROG scan is shown in Fig.2.4a. As seen in the curve of Fig.2.4a the FWHM of this pulse is 82 fs, which is near the transform-limit pulse width mentioned earlier of 79 fs. This is measured after the EOM in the pump line before SHG generation to ensure a short pulse width for maximum SHG conversion efficiency. Once both the pump and probe pulses are introduced into the microscope, it is necessary to ensure that the pulse width at the sample position is compressed for optimal signal and temporal instrument response. To do this we use different FROG techniques through the microscope. For a measurement of the pump pulse at the sample position a method known as co-linear-FROG (cFROG) is used.[1] To do this an interferometer is introduced into the pump line, which splits the beam into two identical beams and one arm is again reflected by a movable stage and both beams are then re-aligned into the microscope. A sample of potassium di-hydrogen phosphate (KDP) is placed on a microscope slide and positioned on the microscope. The two identical, co-linear pump beams are focused onto a KDP crystal, once again producing an SHG signal. The nominal 800 nm light is filtered out with a short-pass filter and the 400 nm SHG signal is focused onto a single-mode fiber and directed into the USB spectrometer. Similar to the signal measurement in SHG FROG, the movable arm in the interferometer is scanned across

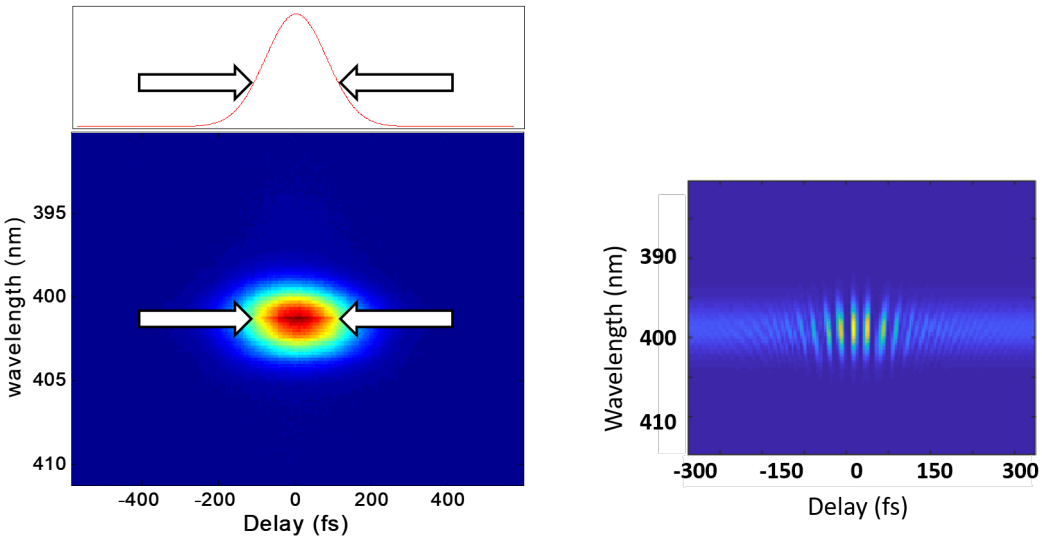

(a) SHG FROG **(b)** cFROG

Figure 2.4: SHG FROG of the pump pulse taken before the BBO crystal in the pump line with a FWHM as indicated by the arrows of 82 fs. **(b)** Representative cFROG scan of the compressed pump pulse at the sample position in the microscope.

the pulse of the stationary arm. However, in cFROG, when the two pulses overlap in time an interference pattern will be observed. An example measurement of cFROG taken on our TA instrument is shown in Fig.2.4b. As seen in this figure the interference pattern only lasts for the amount of time that the two pulses are overlapped and therefore we are able to extract out the pulse width of our pump pulse at the sample position.

In theory the pulse width of the probe line (white light) could be measured in the same manner, however with the much weaker pulse energies, obtaining sufficient SHG intentsity for a FROG measurement is not feasible. Thus, we utilize a different FROG method known as cross-correlation FROG (XFROG).[41] For this method we measure the probe pulse by utilizing one pulse from the probe and one pulse from the pump beam. Again, a KDP crystal is placed at the sample position and both the pump and probe beams are focused onto the non-linear crystal creating a sum-frequency generation (SFG) signal. SFG is a similar process to SHG where two photons of light are absorbed and one photon, at the sum of the two input frequencies, is emitted. The signal measured in XFROG is the sum of frequencies of the 800 nm light plus the wavelength of corresponding white light (500 - 600 nm). This leads to SFG signal centered near 345 nm. The measurement is a convolution of the pump pulse width

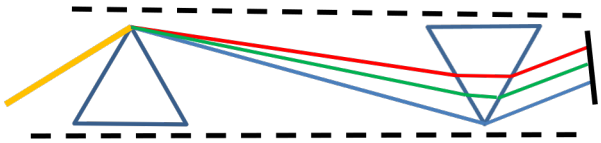

Figure 2.5: Prism compression line showing the parallel configuration of the two prisms and the separation of the different wavelengths with the bluer wavelengths being refracted more than the red wavelengths.

plus the probe pulse width. Now having a known value for the pump pulse, from cFROG, and an overall instrument response time, XFROG, we are able to de-convolve the two and determine the probe pulse width directly. An example XFROG measurement at the sample position in our TA microscope is shown in Fig.2.7. More information and discussion on the optimization of the probe pulse compression and pulse shaping can be found in section **2.2.4**.

2.2.3 Prism Compression

A prism compression line consists of two prisms with the beam passing through each prism twice. Prism lines used in our TA instrument are made with SF-10 glass. The choice of glass that the prism is made out of determines the amount of second and third order dispersion correction that a given prism line is able to compensate for. A material, such as SF-10, that has a high refractive index is able to correct for a higher amount of dispersion in pulse over a shorter distance than a material that has a lower refractive index, such as BK7 glass. An example of a prism compression line is shown in Fig. 2.5.

The first prism in the prism pair will refract the light and begin to disperse the separate wavelengths in space as they travel along some distance. In order to provide maximum transmission through the prism material our prisms are set to a specific angle known as Brewster's angle. The second prism is then set at a specified distance away from the first prism and at the matching angle. Each wavelength of light will then pass through a slightly different path length, traveling at different speeds based upon the refractive index of the material. When set at the correct distance this difference will allow for the pulse to become optimally compressed, or near the FT limited pulse width. When the light first passes through the second prism it becomes collimated and directed onto an end mirror which sends the beam directly back onto itself angling slightly down returning through both prisms. On

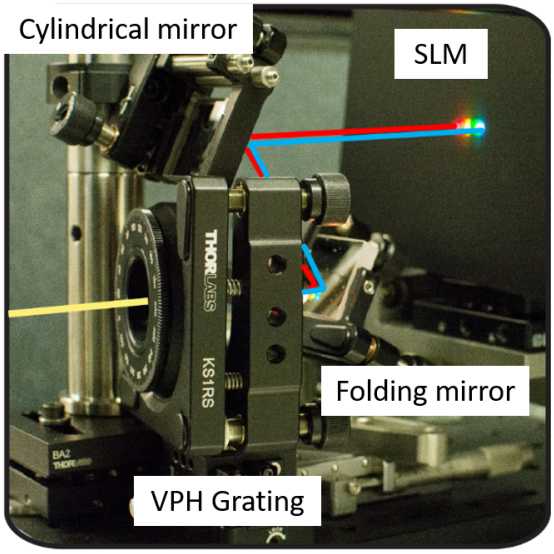

Figure 2.6: Picture of the SLM pulse shaping line, showing the four optics involved and the light path, entering and exiting through the volume phase holographic (VPH) grating.

the second pass of the light through the prism pair, prism two will begin to overlap the wavelengths and the first prism will collimate the beam again with all colors overlapping. If aligned correctly the input and output beams will be identical in space and changed only in the time domain. As seen in Fig. 2.2 we are utilizing a total of four different prism lines throughout the instrument for various reasons. Prism line 1 is for optimal compression of the 800 nm light in order to get favorable white light output from the PCF fiber. Prism line 2 is used for compression, again of the 800 nm light, for optimal SHG efficiency from our BBO crystal compensating for the large amount of dispersion introduced wiht the EOM. Prism lines 3 and 4 are for the pump and probe lines respectively to optimally compress each pulse at the sample position taking into account the microscope objective as well. While prisms are a highly effective method for correcting a large amount of dispersion in a pulse, there are other methods of correcting small amounts or higher orders of dispersion.

2.2.4 Pulse Shaping

In our TA system we have included an SLM-based pulse shaping line in order to correct higher order dispersion in the probe line introduced by the PCF fiber. In order to create a broad white light spectrum, multiple non-linear processes take place in the PCF fiber and thus

introduces a large amount of dispersion in the output pulse. This pulse shaping line consists of four total optics shown in Fig. 2.6; a volume-phase holographic (VPH) transmission grating, a folding mirror, a cylindrical mirror and the reflective SLM. The light will pass through the VPH grating where the wavelengths will be diffracted into several orders. The first order diffraction will be directed, via the folding mirror, to the cylindrical mirror which will then focus the wavelengths in the horizontal dimension onto the SLM face. The SLM face consists of a 600 x 800 liquid crystal display (LCD) where each pixel is 20 μm. The cylindrical mirror is set such that it will focus individual wavelengths to a width smaller than 40 μm, due to constraints on the system and strong aberrations in the light, a smaller spot size was not realistic or necessary for our system. Behind the LCD screen is a reflective face which sends the light back on its incoming path to the cylindrical mirror to re-collimate the light back through the VPH grating which then spatially overlaps all wavelengths again. Initially, the beam is unaltered in time as there is no phase applied to the LCD screen on the SLM. As seen in Fig. 2.7**(A)** the bluest and reddest wavelengths are arriving at the sample at approximately the same time while the middle wavelengths are arriving at a different time. This is due to a higher order dispersion present in the probe pulse. This can be fixed by applying a separate phase to each wavelength on the SLM face. The overall phase of the probe pulse is determined by a FROG algorithm. This phase is then incorporated into a custom LabView program and converted into gray-scale so that it can be applied to the LCD screen on the SLM. This will allow for the liquid crystals to rotate in and out of the direction of light polarization and change the refractive index that each wavelength sees. This will essentially 'speed up' or 'slow down' certain wavelengths relative to the others. In theory this will allow for the exact phase of the pulse to be fixed and have an optimally compressed broadband probe pulse. As seen in Fig. 2.7**(B)** the pulse width of the phase corrected XFROG is much shorter overall and is nearing the transform limit. This pulse is, however, a convolution of the pump and probe pulse widths and is therefore limited by the pump pulse of approximately 80 fs.

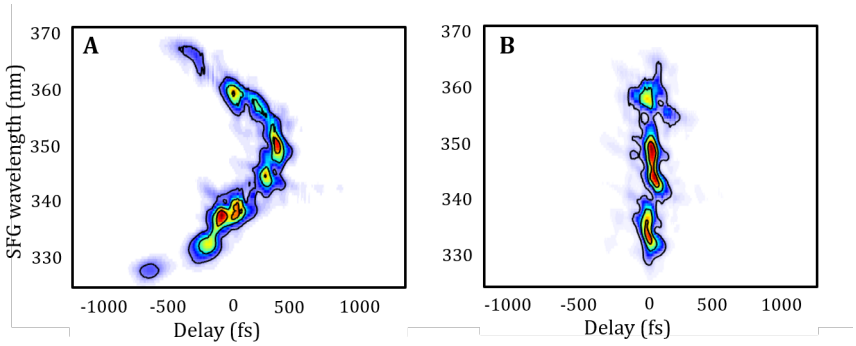

Figure 2.7: XFROG traces of the (A) uncompressed and (B) compressed probe pulse from the output of the PCF fiber.

2.3 Modulation

As seen in Fig. 2.2, the pump beam is directed through an electro-optic modulator (EOM). The output of the Ti:Sapphire oscillator has a repetition rate of 80 MHz and after passing through the EOM is modulated to 26.7 MHz. As mentioned previously, the pump pulse is modulated for use with lock-in detection of our TA signal. The TA signal is achieved at the same wavelength as the probe beam, in order to separate the two they must be at different repetition rates. Now that we have modulated our pump beam, our signal will also only be achieved at the repetition rate of the pump and at the wavelength of our probe beam. Therefore, a reference frequency is also transferred from the EOM counter to the lock-in amplifier at the 26.7 MHz frequency in order to isolate the desired signal from the probe beam. An EOM is a device which is able to control the amplitude of a laser beam with a high voltage electrical signal. The EOM consists of a nonlinear medium (such as ammonium dihydrogen phosphate ADP) which an electric field is applied to, to alter the polarization of the input laser beam. This is followed by a calcite polarizer at the output of the EOM which then rejects the light that has been changed in its polarization. A separate counter device initially takes in a reference reading of 80 MHz from the oscillator and is set to divide that frequency by three giving the output frequency of 26.7 MHz which is then sent to the EOM driver as a reference frequency. The driver then sends the electrical signal to the EOM at the desired frequency and set to a specific voltage for optimal modulation efficiency of the laser beam.

2.4 Microscope Components

In addition to the short temporal resolution, a low spatial resolution is also necessary to take time-dependent TA measurements on samples in the single-micron range. The microscope base used in our setup is an Olympus IX73 with an Olympus 100X, 1.4 NA objective for focusing. The light is directed into the microscope through a side port where it is then directed to the objective with a silver mirror. The beam size at this point is large enough to sufficiently overfill the back aperture of the objective by approximately a factor of two. This is done to be sure to fully utilize the full NA of the objective being used. The NA of the objective is the angle of the 3D 'cone' of light being focused to a spot on the sample. An objective with a high NA (1.4) has a steeper angle of focusing when compared to an objective with a lower NA and therefore focuses to a smaller spot size. The NA is calculated from a plain-wave and therefore by overfilling the back aperture of the objective with a Gaussian wave, we are coming close to the approximation of a plain wave entering the objective and can consider the difference negligible.

When using a high NA objective for focusing our light onto our sample we are able to achieve a low spatial resolution that is diffraction limited. The lateral resolution for an objective with an NA > 0.7 is given by the equation:

$$R_{lat} = \frac{0.383\lambda_{ex}}{(NA)^{0.91}} \tag{2.2}$$

And the axial resolution for the same system is give by the equation:

$$R_{axial} = \frac{0.88\lambda_{ex}}{n - \sqrt{n^2 - NA^2}} \tag{2.3}$$

In our system, when utilizing a 400 nm pump pulse, λ_{ex} is 400 nm, and the NA is 1.4 giving us a theoretical lateral resolution of 113 nm and an axial resolution of 376 nm when using the refractive index of our immersion oil (n = 1.515). TAM is a point-scanning technique, meaning that the laser is focused to a small spot on the sample and either the laser or the sample must be raster scanned in order to build up an image. For the studies presented here an X,Y,Z scanning stage was utilized in order to raster scan the sample across

the laser beam and collect the resulting signal. The TA signal achieved in our system is in a transmitted direction and must be collected with a second high NA objective above the sample. In order to collect the maximum amount of signal, ideally a collection objective with an NA equal to or higher than the focusing objective's NA should be utilized. For a majority of our measurements the light collected was focused onto a single mode fiber which transferred the light onto our detector.

2.4.1 Sample Position

For all of our spectroscopy and a subsection of the imaging studies, it was necessary to utilize a flow cell at the sample position in the microscope. This normally would be a trivial problem and a commercial flow cell would be available for use. However, with the use of 1.4 NA focusing and collection objectives and their short working distances (0.13 mm), a custom-built flow cell was necessary. We attempted to utilize multiple commercial flow cells that allowed coverslips as the top and bottom layer of the cell, but found that the thickness between the coverslips was too large to use the necessary objectives. Instead, we constructed a custom flow cell that fit our exact needs. A construction diagram of the custom flow cell is shown in Fig. 2.8. A standard thickness (1 mm) 3 x 2 inch microscope slide was used for support purposes and bonded to a 3 x 2 inch coverslip via polydimethylsiloxane (PDMS) in a plasma cleaner. As shown in the diagram the support glass has a 0.75 x 1 inch hole cut in the middle to allow the oil immersion objective to reach the coverslip while leaving ample room to navigate the sample area. The support glass was then plasma bonded to a 250 μm PDMS sheet cut to the same dimensions as the glass. The coverslip was then also plasma bonded to the opposite side of the PDMS sheet effectively connecting the coverslip and support glass. After connecting the two pieces of glass, two small holes (1/16" diameter) were drilled through all three layers of material which will later be used to flow the sample through. The flow channel was cut from double stick tape to the desired dimensions. Typically, a flow channel was cut from a solvent-resistant tape with a thickness of approximately 170 μm, with a channel width of 5-7 mm and a length of 5.5 - 6 cm. The double stick tape is placed on the coverslip with the bottom half of the tape then covered with a second 3 x 1 inch coverslip creating the flow channel between two coverslips with a thickness matching the

Table 2.1: Commercial flow chambers and double stick tapes used for the custom flow cell.

Flow cell / Tape brand	Chamber Thickness (mm)	Part Number
PeCon Perfusion Chamber	0.350	POC-R2
Grace Biolabs Perfusion Chamber	0.350	622302
3M Solvent Resistant Tape	0.170	7602A53
3M Adhesive	0.050	3M 9969
3M Adhesive	0.025	3M 467MP

chosen tape. The different double stick tapes, commercial flow cells and their corresponding channel thickness are shown in Table 2.1. For solutions the flow cells were used as is, and when applied for imaging of cells and beads further measures were taken to immobilize the beads and yeast cells. For imaging of polystyrene beads (Chapter 3), an avidin coverslip was used as the bottom of the flow cell. For live yeast cell imaging (Chapter 4), 10 μL of a 1:1 solution of 2 mg/mL concanavalin A and 0.1% poly-L-lysine was spread onto the coverslip and dried for 10 min before being applied as the bottom half of the flow cell.

2.5 Discussion

The current TA microscope has been constructed and utilized for preliminary studies (Chp. 3 4). As discussed above, it has been constructed initially with a scanning stage for image acquisition. This limits the total image acquisition time to a few seconds per image, depending on the size of image being acquired. Laser scanning mirrors can circumvent this issue and allow for a similar size image to be acquired in the sub-millisecond range. Laser scanning mirrors have been built and tested on the system, and are a possibility for improvement. The current limitations of the instrument are dealing with a sample which produces a signal-noise ratio high enough for faster scanning. With changes in our media

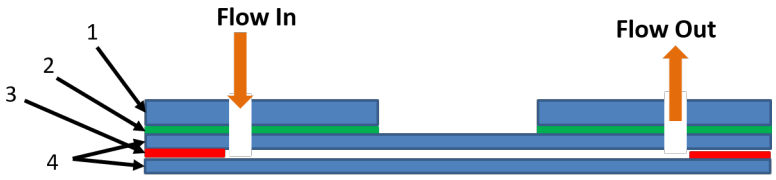

Figure 2.8: Diagram of the center section of our custom flow cell. 1) Support glass slide, 2) PDMS layer, 3) double stick tape, and 4) coverslips.

being used, and changes in how we are preparing the samples we should be able to improve upon our current S/N limitations (more discussion in Chp. 4). Our scanning mirrors consist of a resonant and non-resonant mirror with which scanning rates can easily be pushed to video rate (30-60 Hz). The resonant scanning mirror scans at a rate of 8 kHz which would allow full images of pixel size 126 x 126 or 256 x 256 to be acquired on the order of milliseconds as opposed to the current time of minutes. This would be a great asset if at some point we were able to monitor the small molecule to membrane interactions in real time on living cells.

Chapter 3

TAM Applications

A version of this chapter was originally published by Kevin Higgins and Tessa Calhoun in *Optics Letters*.

Kevin Higgins, Tessa R. Calhoun. "Compressed supercontinuum probe for transient absorption microscopy." *Opt. Lett.* **2018**, 43(8):1750 - 1753

3.1 Abstract

Here, we combine three optical advancements to transient absorption microscopy in order to access the photodynamics in systems requiring stringent spatial and temporal resolution criteria. First, a broadband visible probe is generated by a commercial photonic crystal fiber. Second, a spatial light modulator-based pulse shaper is incorporated to reduce the pulse dispersion and improve temporal resolution. Third, 1.4 numerical aperture objectives for excitation and light collection provide optimal spatial resolution. The result of these improvements is a probe beam that spans 115 nm across the visible region yet maintains a 100 fs instrument response at the sample position. We demonstrate the capabilities of this microscope by imaging polystyrene beads in a solution of IR-144 dye, revealing aggregated species at the bead surfaces.

3.2 Compressed supercontinuum probe for transient absorption microscopy

The ability to measure ultrafast processes governing excited state evolution has dramatically aided in our understanding of a wide range of chemical and physical phenomena, including solvation [35], photosynthetic energy transfer [5], and the photophysics of new materials [42, 17, 3]. Within the last decade, this capability has been adapted onto a microscopic platform allowing the imaging of nonfluorescent species in biological systems [24, 40, 43, 49, 63], direct visualization of energy flow in solar materials [29, 60], and characterization of pigments in historic artwork [68], to name just a few applications. Universal to these applications of transient absorption microscopy (TAM) are the use of two ultrafast laser pulses, the first to promote a molecule of interest to an excited state and the second to probe the transient populations. By varying the delays between the two pulses, one can measure the states lifetime and track energy and decay pathways [16, 27, 48, 23]. The resulting information provides insight not only into the electronic structure of the system itself, but also reflects changes in the systems interaction with its local environment. This makes TAM a powerful approach for chemical imaging where changes in local chemical composition or interactions can be mapped using intrinsic ultrafast events as chemical contrast [16, 27, 23]. In most ensemble TA spectroscopy experiments, a relatively narrowband pump pulse is used to excite a single electronic transition, while a broadband probe, often produced via sapphire supercontinuum, interrogates a wide energetic window. The resulting signals are spectrally isolated and simultaneously detected using a spectrometer. While this approach has been successfully applied to microscopy [58], it is not without limitations. Most importantly, pushing the limits of spatial resolution in order to understand complex, heterogeneous systems requires the use of high numerical aperture (NA) objectives and increasingly small sample volumes. This necessitates operating in the MHz repetition rate regime with lock-in detection to obtain an acceptable signal-to-noise ratio on the resulting images [16,17]. As such, it is most common in TAM measurements to use optical parametric oscillators (OPOs) to produce a tunable probe pulse. The use of OPOs, however, introduces the requirements that the laser be separately tuned to probe different transient states, in contrast to ensemble

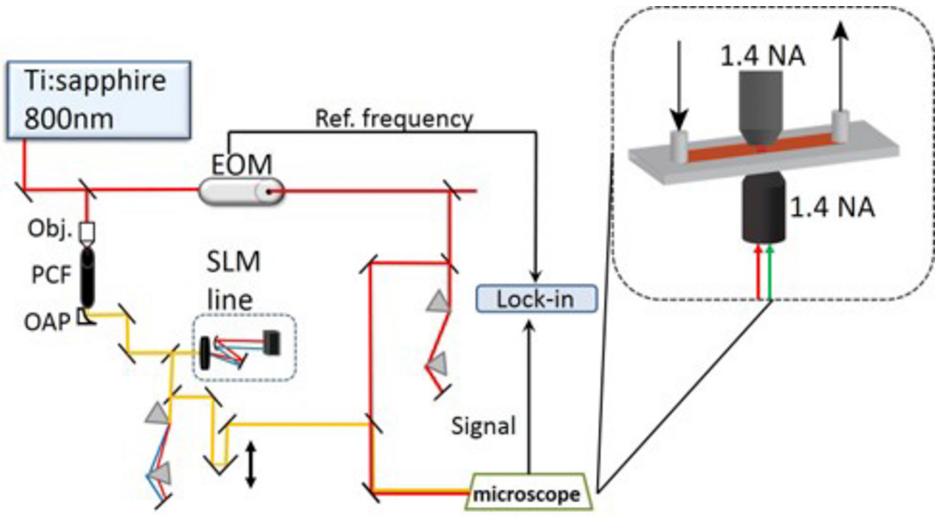

Figure 3.1: Experimental layout of the transient absorption microscope. EOM, electro-optic modulator; Obj, objective; PCF, photonic crystal fiber; OAP, off-axis parabolic mirror. Top right inset, microscope sample position with high NA focusing and collection objectives on either side of a flow cell.

spectroscopy, and restricts the ultimate temporal resolution limit due to their narrowband output. OPOs also add significant cost to the experimental apparatus.

As an alternative to OPOs, supercontinuum generated by photonic crystal fibers (PCFs) has been proven to be a useful probe for TA spectroscopy [39, 12, 32] and microscopy [45]. PCFs have been shown to be capable of producing an octave-spanning supercontinuum with low energy input that can be provided with a high-repetition-rate laser, making them ideal for use with readily available and low-cost ultrafast oscillators [21]. The previous applications of PCFs to TA experiments, however, used the raw output of the fiber, which is many ps long and limits the temporal resolution of the instrument. In parallel, multiple groups have demonstrated the ability to compress PCF supercontinuum output in microscopes with high NA objectives, but their fibers were limited to near-infrared (IR) wavelengths, which restricts the systems that can be studied [70, 66]. All-normal dispersion PCFs have been introduced to provide compressible supercontinuum pulses [32], but they are either custom fibers or again limited to the near-IR. There are multiple advantages to utilizing a commercially available, sealed PCF: ease of mounting and alignment, optically cleanable facets, reduced cost, and increased longevity of the fiber compared to bare PCF fiber. Here, we demonstrate the compression of a PCF-generated *visible*,broadband supercontinuum probe at the focus of a

high-NA objective and its application to resolving spatial heterogeneities with TAM using temporal responses as chemical contrast.

The TA microscope used in this study is depicted in Fig. 3.1. It uses a Ti:sapphire oscillator (Mai Tai, Spectra Physics) to produce pulses centered at 800 nm with an 80 MHz repetition rate. The output is split into two arms, a pump and probe, where the pump beam is modulated using an electro-optic modulator to 26.7 MHz for lock-in detection. The supercontinuum probe beam is generated by focusing 3.5 nJ of the 800 nm pulses into the PCF (SCG-800-CARS, Newport) using a 40X objective. The broadband output is collected and collimated using an off-axis parabolic mirror. Probe compression is achieved with both a prism line and a liquid-crystal spatial light modulator (SLM)-based pulse shaper [71]. This pulse-shaping line has been adapted from previous work with some modifications [67, 11]. Briefly, the line consists of four optics: a volume phase holographic transmission grating, a folding mirror, a cylindrical mirror (f = 100 mm), and a reflective SLM. The SLM consists of a 600 800 array of liquid crystals with a pixel size of 20 m (Hamamatsu). This configuration, with a two-dimensional SLM array, allows for both amplitude and phase shaping, although the experiments reported here rely exclusive on the application of phase. The pump and probe beams are finally combined using a dichroic mirror before being sent into the microscope where they are focused with a 100X 1.4 NA oil immersion objective (Olympus) onto the sample. The samples are raster scanned using a scanning microscope stage. The signal is collected in a transmitted direction using a second objective, spectrally isolated using a combination of filters, and sent to a single pixel avalanche photodiode. The signal is finally isolated using a lock-in amplifier and read out on a computer using custom LabVIEW codes.

The generation of blue frequencies from PCFs is a longstanding challenge [25, 34, 38], and the PCF used in our work is one of the few commercially available fibers that produces a supercontinuum spectrum extending significantly into the visible region. Theoretically, the output of the PCF has a spectral range of ¡600 nm to ¿1200 nm, largely dependent on the input parameters of pulse width and energy [33]. For our experiments, 115 nm of visible wavelengths, 560675 nm (Fig. 3.2(C)), are selected from the fiber supercontinuum and introduced into the microscope. The nonlinear processes taking place in the fiber to

produce the spectrum introduce a large amount of dispersion leaving the output pulse at nearly 1 ps (Fig. 3.2(A)) even after prism compression. In addition to its visible spectrum output, this fiber also has the benefit of not relying on soliton fission for spectral broadening [33]. This property reduces the noise of the output and retains the pulse coherence necessary for compression [33, 30].

To characterize the temporal and spectral characteristics of our supercontinuum pulses, cross-correlation frequency resolved optical gating (XFROG) [41] experiments were performed at the sample position in the microscope using potassium dihydrogen phosphate (KDP) crystalline powder grains as a nonlinear up-conversion media. Figure 3.2(A) shows an XFROG trace collected with zero phase applied to the SLM. The sum frequency generation signal between the pump and probe pulses was collected with a 40X 0.5 NA UVB objective (LMU-40X-UVB ThorLabs), and spectrally resolved with a USB spectrometer (Maya, Ocean Optics). The 800 nm pump pulse was compressed to 85 fs at the sample position with a prism pair as confirmed by cFROG [1] (data not shown). The ¿1000 fs duration of the signal in Fig. 3.2(A) therefore predominantly arises from the uncompensated phase on the probe pulse. The prism compression line corrects a majority of the second-order dispersion, leaving a large third-order component. In order to extract the exact phase needed for compression, the data in Fig. 3.2(A) were processed with the FROG algorithm [41, 64]. This phase is then fit to a high-order polynomial, which is in turn applied to the SLM. The use of a polynomial fit eliminates any discontinuities in the extracted phase that can induce unwanted aberrations in the pulse if applied to the SLM directly. Figure 3.2(B) shows the XFROG data collected when this extracted phase is corrected using the SLM. The full width at half maximum (FWHM) of this data is reduced from over 1000 fs to ¡105 fs (Fig. 3.2(D)) with the remaining major contribution due to the pump pulse width of 85 fs. In fact, the duration of the probe pulse alone is estimated to be 53 fs as extracted from the FROG algorithm. The remaining deviation between this value and the transform limit likely arises from the inability of the polynomial fit to reproduce the exact phase necessary for correction. It is expected that further optimization could be achieved by the addition of phase corrections extracted from data in Fig. 3.2(B). Figure 3.2(C) shows that the entire 115 nm of bandwidth introduced to the sample through the 1.4 NA objective (red trace) is preserved after the

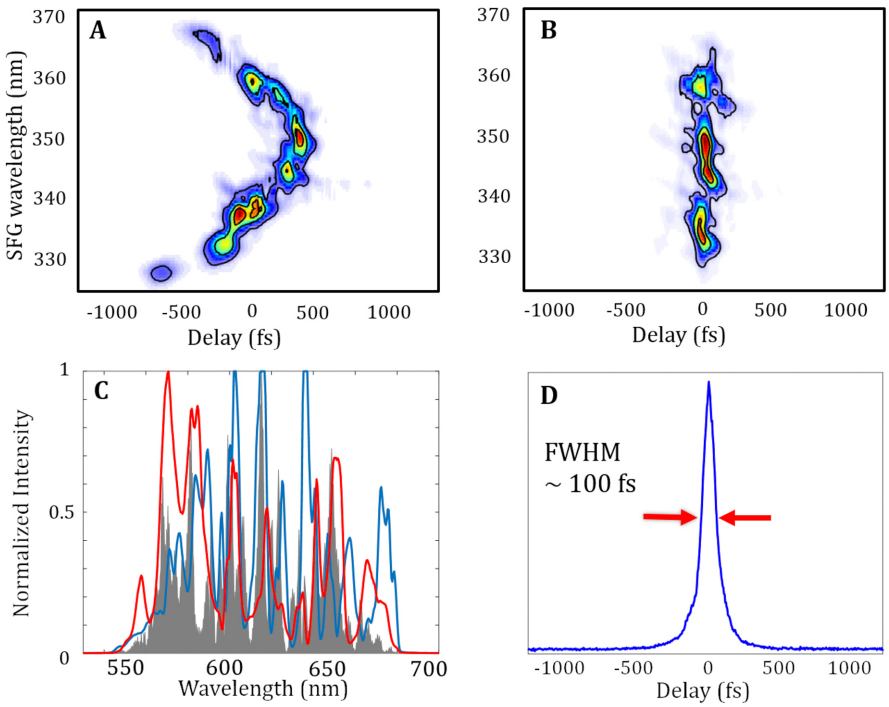

Figure 3.2: XFROG traces of the uncompressed (A) and compressed (B) PCF supercontinuum output. Spectra at the sample position (C) with (blue) and without (red) phase applied to the SLM and the recovered spectrum from FROG (gray). Temporal profile of the compressed XFROG with a FWHM of 100 fs (D).

addition of the phase (blue trace) and recovered by the FROG algorithm when applied to the compressed XFROG data. In order to demonstrate the spatial and temporal capabilities of the compressed PCF-based TA microscope, we have imaged polystyrene particles in a solution of IR-144 dye. Commercial polystyrene particles (0.70.9 μm) coated with biotin were purchased from Fischer Scientific and subsequently diluted 1:1000 in a phosphate buffer solution. Particles were then immobilized on a commercial avidin coated coverslip. This coverslip with the immobilized particles is applied as the bottom half of our homebuilt flow cell with a second coverslip as the top half. The TA signal is collected using a 60X 1.4 NA oil immersion objective (Nikon). The dye solution was flowed over the beads in order to dissipate any local heating damage caused by the incident laser beams.

IR-144 has previously been studied via TA spectroscopy[50], and its aggregation at interfaces has been reported [59]. Figure 3.3, however, shows the first application of TA microscopy to this system directly linking the spatial and temporal behaviors in a single

experiment. A 200 μM solution of IR-144 in methanol was flowed through the sample cell. The path length of the flow cell is estimated to be 140 μm based on thickness of the tape used between the coverslips. A 375 pJpulse pump beam at 800 nm was used to excite from the ground state to the first excited state of IR-144. The ground state bleach signal was then monitored with a 12.5 pJpulse probe beam centered at 600 nm. TAM images are shown in Fig. 3.3(A) at an interpulse time delay, $\Delta\,\tau$, of 2 ps and took approximately 10 min to obtain. This image clearly shows a distinct signal arising from IR-144 around the beads (white), and the bulk solution (gray), whereas the polystyrene beads appear as black regions, since they do not have an optical response in this spectral region. To further confirm the source of the signal, a TAM image has also been acquired at a $\Delta\,\tau$ of 12 ps (Fig. 3.3(B)) when the probe precedes the pump. As expected, the contrast arising from the transient states of IR-144 is no longer apparent. A line profile across the bead edge is shown in Fig. 3.3(C). A sigmoidal fit of this data is shown and estimates the lateral resolution of our instrument as 414 nm [15].

It is evident in Fig. 3.3(A) that there is an accumulation of dye molecules, or an enhanced optical response, at the surface of the polystyrene beads. Based on previous ensemble spectroscopy work, it was surmised that aggregation at the particle interface results in notably different dynamics of IR-144 as opposed to species in the bulk solution at the same concentration. To more directly illustrate that the species at the surface are aggregated, we collected the ultrafast temporal dynamics at two spatial regions in Fig. 3.3(A). This information is available only using the intrinsic ultrafast time resolution in conjunction with high spatial resolution afforded by the compressed PCF-based TA microscope. The time traces are shown in Fig. 3.3(D). Each decay measurement took approximately 20 min to acquire and the high signal-to-noise ratio suggests that the supercontinuum stability is suitable for these types of experiments. The blue x markers were obtained from the marked region in Fig. 3.3(A) at the surface of the particle where the dye is appearing to accumulate. The response from the bulk solution away from the particles, shown in red, displays notably different dynamics, indicating different local chemical environments, most likely due to different aggregation states. By fitting each of the curves to a single exponential we are able to extract the excited-state lifetimes from these different environments. For the

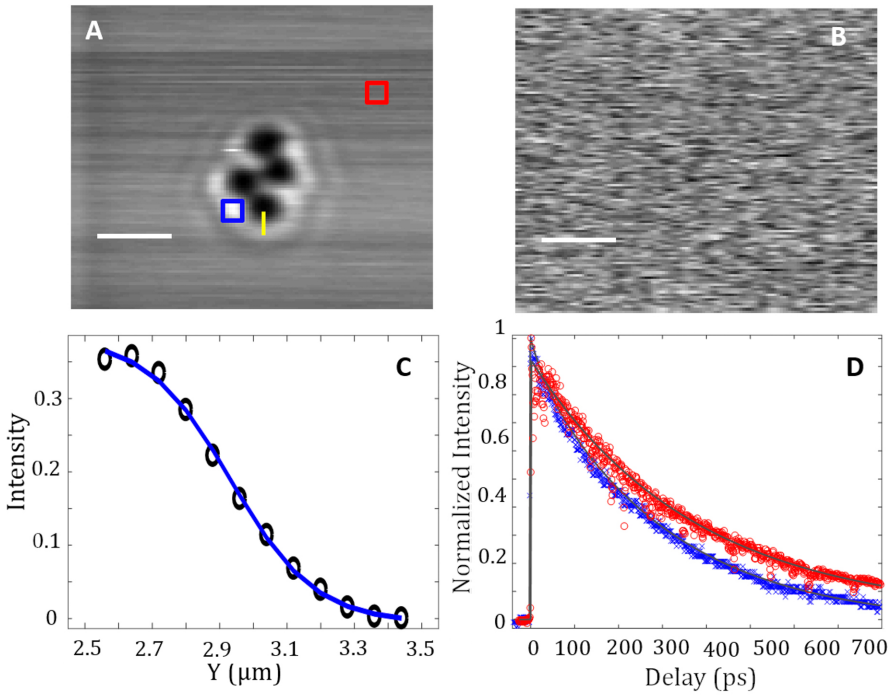

Figure 3.3: Transient absorption images of 200 M IR-144 solution flowing over 0.70.9 m polystyrene particles. (A) TAM image taken at $\Delta\ \tau$= 2 ps; (B) TAM image of the same region with $\Delta\ \tau = 12$ ps. (C) Line profile taken from image (A), as shown by the yellow line. Data are represented by dots, while the solid trace is the fit. (D) TA time-decay of IR-144 and the indicated areas from the image in (A). Scale bars are 2 μm.

monomeric solution of IR-144, the time decay results in a 321 ps lifetime, while the dye near the edge of the particle is significantly shorter at 189 ps. In addition to facilitating the use of PCFs for TAM experiments requiring optimal temporal resolution, the approach developed in this work can easily be expanded to other nonlinear microscopy techniques in the visible spectrum with minimal instrumental modifications. For example, the pulse shaper can be used to generate two different colored pulses from the supercontinuum for pump-dump-probe experiments [37] on spatially heterogeneous samples. Similarly, pulse trains could be generated for optical Kerr effect measurements [54], or the probe polarization itself can be shaped [8]. It is expected that with the flexibility afforded by a whitelight probe pulse and pulse shaper in a high NA microscope, that these advances will impact a broad range of fields beyond those demonstrated here.

This work demonstrates the compression of the visible supercontinuum from a commercially available PCF using an adaptive pulse shaper for use in high-repetition-rate TAM.

Through optimal pulse compression, a temporal resolution of 100 fs is achieved at the sample position of a high-NA microscope. We demonstrate the utility of having both this high temporal resolution and probe wavelengths in the visible spectral window by imaging the aggregation and dynamics of IR-144 at polystyrene nanoparticles. These images reveal that aggregation of IR-144 at the surfaces produces distinct dynamics, and show that TAM is uniquely sensitive to imaging differences in chemical environments. Continued work using compressed PCF-based TAM is aimed at imaging non-emissive species in complex matrices leveraging the high joint temporal and spatial resolutions of the present instrument.

Chapter 4

Amphotericin B Imaging

4.1 AmB Review

Amphotericin B (AmB) is an anti-fungal drug that has been in use since the 1950's and has a high rate of cell death with minimal reports of developed resistance. The drug is on the World Health Organization's list of essential medicines.[46, 10] However, it does have some very serious side effects, including; fever, chills, kidney failure and death. The structure of AmB is shown in Fig. 4.1; it is known as a polyene antibiotic owing to its long conjugated backbone. This conjugation is responsible for the absorption of visible light near 400 nm. There are currently a few less toxic alternatives being used in lieu of AmB, however most are not as effective and have seen significant amounts of resistance developed. Due to AmB being highly insoluble in water, and highly soluble in lipid solutions, AmB is a great candidate for lipid-based formulations.[14] These formulations have been shown to have reduced toxicity but also reduced fungal cell death efficiency.[44] The combination of these factors is what has lead to AmB's continued use as a last line of defense for serious fungal infections, after other less toxic alternatives have been tried.[62, 51] It is commonly accepted that the drug interacts and possibly disrupts the membranes of fungal cells leading to cell death, however, the mechanism of action (MOA) for this drug is highly debated due to contradictory studies on the matter. It would be beneficial to determine the MOA for this particular drug due to it being highly effective and having minimal reports of fungal resistance. If we can determine the MOA for AmB this information could possibly lead to new drug designs that more

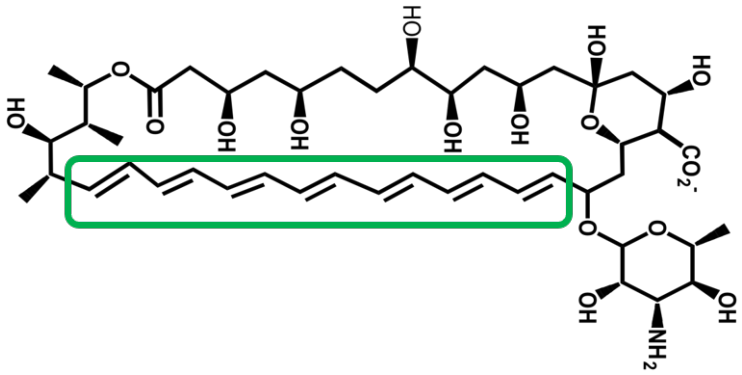

Figure 4.1: AmB Structure where the chromophore backbone is outlined in the green rectangle.

efficiently target fungal cells and reduce toxicity. Currently there are three prominent MOAs that have been proposed for AmB. The first and most widely accepted MOA is known as the ion-channel formation (Fig. 4.2**C**).[22] The next MOA being a sponge-model formation (Fig. 4.2**A**)[2], and the last MOA involves monomer AmB molecules penetrating the cell membranes and undergoing processes to cause radical oxidative damage to the cells (Fig. 4.2**B**).[61]

The ion channel formation MOA involves the AmB molecules inserting into the membrane where it will also bind with ergosterol molecules and become aggregated to span across the lipid bi-layer as shown in Fig. 4.2 **C**. When spanning the bilayer the AmB molecules form a pore where small ions, such as K^+, Ca^{2+}, and Mg^{2+}, begin exiting the cell leading to loss of cellular function and eventually cell death. Even though the ion channel mechanism is the oldest and perhaps the most accepted MOA of AmB, conflicting studies have shown there to be a large out-flux of ions from the cell with the cell still functioning for some time after.[61] While this MOA has evidence it is occurring, it may not be the only mechanism which is leading to cell death.

In a second MOA, it is proposed that AmB attacks fungal cells, which is known as the 'sterol sponge' model, shown in Fig. 4.2 **A**. In this model the AmB molecules aggregate on the outside of the membrane and form a sponge-like structure in which they begin extracting ergosterol from the membrane. With the ergosterol extracted from the membrane, certain cell processes can no longer function and will eventually lead to cell death.[55, 31, 53] This MOA was determined through a combination of electron microscopy and spectroscopy studies.

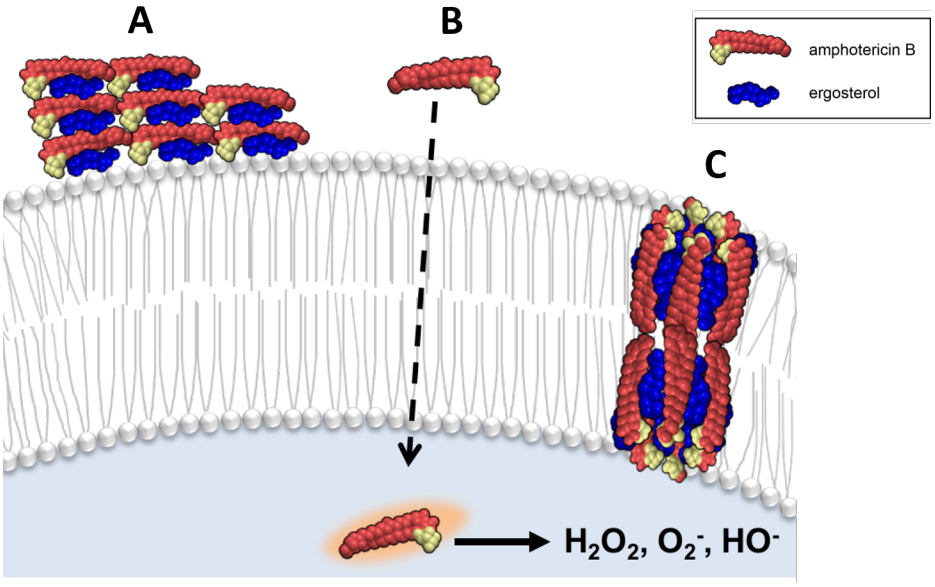

Figure 4.2: Three proposed mechanisms of action for AmB showing (a) ergosterol containing sterol sponge, (b) monomer internalization and creation of radical oxygen species, and (c) ion-channel formation.

Anderson et. al. observed large AmB aggregates on the exterior of model membranes via electron microscopy. The model membranes were, however, composed of a relatively simple composition and a much lower ergosterol concentration than is present in fungal systems. This combined with the considerably higher kinetic barriers hindering ergosterol from exiting the living membranes, poses significant concerns about this MOA as well.[36]

In a third proposed MOA for AmB, the drug molecules are internalized into the fungal cells as monomers (Fig. 4.2 **B**). AmB is thought to penetrate the membrane, where it then undergoes oxidation and begins to produce harmful radical species within the cell.[61] The radical species within the cell have been detected before significant membrane damage has occurred via pore formation or other possible processes.[57] Each of the three described MOA for AmB leading to cell death and its antifungal properties are plausible and supported by multiple research studies. However, each of them also contain contradictory information and possible alternatives. It then becomes clear that it is necessary for further investigation on the interactions of AmB and fungal systems in the least invasive way. For this reason we have chosen to utilize TAM to image AmB molecules interacting with living yeast cells in a label free manner. From the images obtained with TAM, we will be able to identify if

the AmB molecules are being internalized versus membrane bound, and we will be able to identify localization and distribution of the AmB in either location.

4.2 TAM imaging of AmB

We utilized TAM in order to image native AmB interacting with live yeast cells. As noted earlier, a pump pulse at 400 nm was utilized for initial excitation of the AmB molecules and a probe pulse centered around 550 nm was used to stimulate the TA signal giving our image contrast. The 400 nm pump pulse was chosen based partially on the absorption spectrum of AmB and partially on the ease of use of the available laser wavelengths. The probe wavelength is not as straight forward to be chosen, because there are very few excited state spectroscopy studies performed on AmB previously. One such study was a fluorescence lifetime study of AmB in water to study the lifetimes of the excited states.[28] They found that depending on the emission wavelength observed and the aggregation state of the AmB, varying lifetime components could be measured. As a monomeric solution a shorter lifetime of 10 ps and a longer component of 350 ps was observed. We based our initial probe wavelength on TA spectroscopy studies performed on the carotenoids, β-carotene and zeaxanthin.[6] This is possible due to the similarity of the polyene backbone present in both carotenoids and AmB, differing only in the length of conjugation. With the excited state spectrum of zeaxanthin combined with our available probe wavelengths, preliminary studies were performed on solutions of AmB to determine that 550 nm is near the ideal wavelength range for TAM imaging. Representative spectroscopy scans of AmB solutions are shown in Fig. 4.3. This data shows a time trace of 100 μM AmB in DMSO with detection at both 505 nm (red trace) and 550 nm (blue trace). As is seen in the figure, the 505 nm scan has an initial strong spike followed by a quick decay when compared with the 550 nm scan where it is a more consistent signal and a slower decay. The exponential fits for both decays are also shown in Fig. 4.4 with the fit for 550 nm probe on the left and 505 nm probe on the right. The 550 nm probe signal was fit to a single exponential decay with a lifetime of 1.2 ns while the 505 nm signal was fit to a double exponential with a shorter lifetime component of 2.1 ps and a longer component of 287 ps. While the lifetimes that we have measured for the different

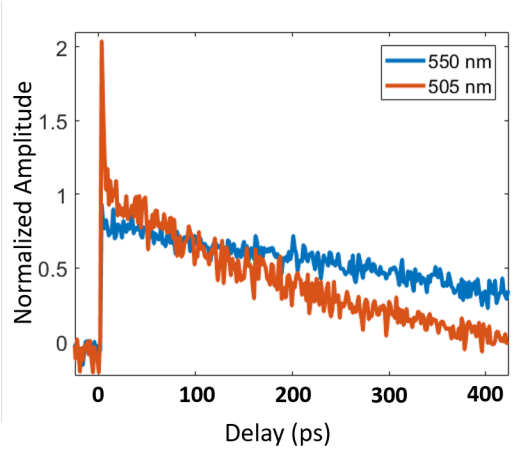

Figure 4.3: TA time decay of 250 μM AmB in DMSO with detection at 505 nm (red) and 550 nm (blue).

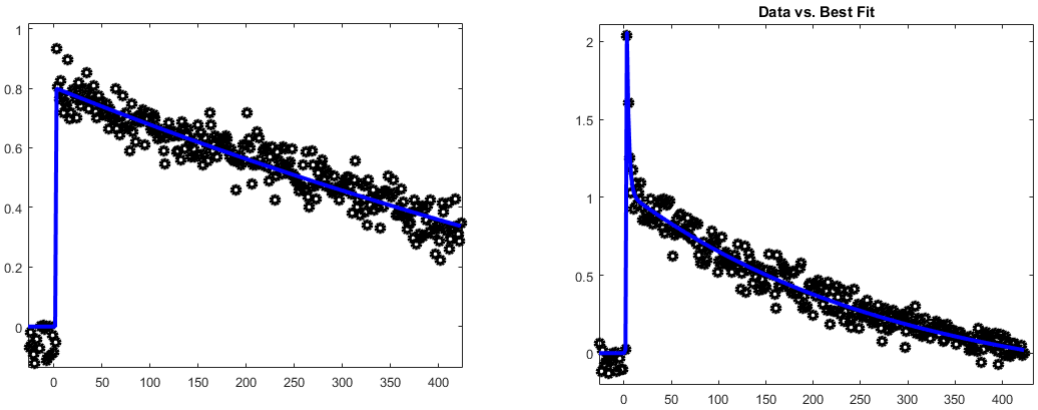

Figure 4.4: Exponential decay fits of 250 μM AmB in DMSO with detection at 550 nm (left) and 505 nm (right)

wavelengths do not match the previous fluorescence lifetime measurements mentioned earlier, our studies were performed in a solution of pure DMSO whereas theirs were performed in water at differing pH levels. This could likely lead to a different environment for the AmB molecules and altering the excited state structure. However, they are similar in that we have measured both a faster and longer component lifetimes adding to the assumption that the solvent is making a difference.

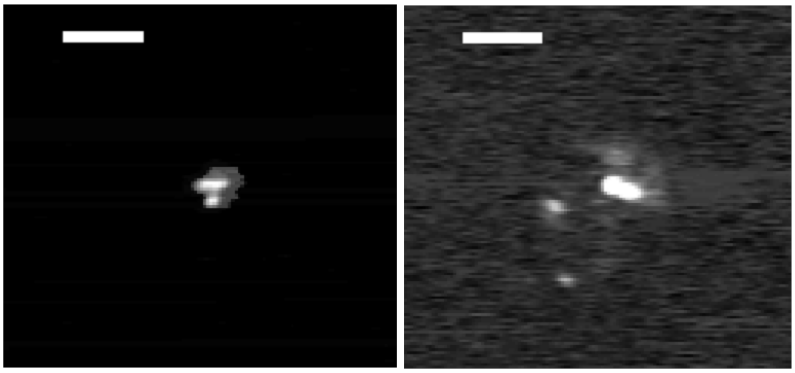

Figure 4.5: TAM images of AmB (50 μM) interacting with live yeast cells. Taken approximately 90 min after AmB introduced to the cells. Scale bars are 2 μm.

4.2.1 Sample Preparation

Initially yeast cells were grown overnight in yeast peptone dextrose (YPD) media at 30 °C. The overnight stock was then diluted 1:50 and grown to log phase (4-5 hours). A small aliquot (500 μL) of cells was taken from the stock and incubated for various times with differing amounts of AmB. Initially AmB was introduced as a monomer in a solution of DMSO to a final concentration ranging from 50 - 250 μM and incubated at 30 °C between 30 - 90 min. Once the cells were incubated for the desired amount of time approximately 7 μL of the yeast/AmB solution was immobilized onto a coverslip and placed onto the microscope for imaging. The cells were immobilized on the coverslip with 10 μL of a 1:1 solution of 2 mg/mL concanavalin A and 0.1% poly-L-lysine spread onto the coverslip and dried for 10 min. The cells were then 'sandwiched' with a second coverslip to be used in the microscope. For the initial studies this was the only prep to the samples and they were imaged over a period of 2 - 3 hours. In later studies, some yeast samples were immobilized onto a coverslip which acted as the bottom chamber of a flow cell as described in Chapter 1. Having a flow cell allowed us to introduce AmB at known times and begin to monitor the interactions immediately.

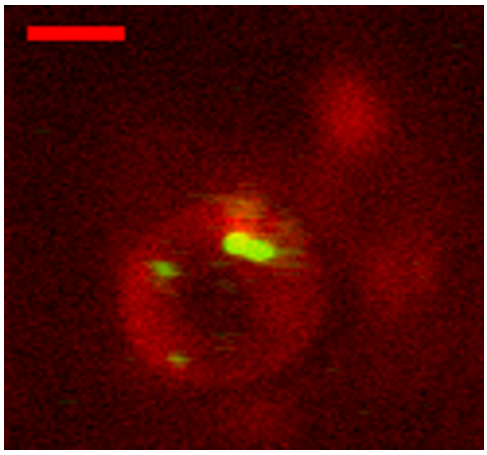

Figure 4.6: TAM image of AmB in YPD at 50 μM taken 90 min after AmB introduced. Red signal is autofluorescence and the green signal is arising from TA. Scale bar is 2 μm.

4.2.2 Results and Discussion

Using the transient absorption microscope described previously and the above sample preparation, promising TAM images were collected from AmB incubated with living *Saccharomyces cerevisiae* cells (Fig. 4.5). Cells were incubated with 50 μM AmB in DMSO for 60 min before immobilization onto the coverslip. The images were collected with a time delay of 200 fs. Fig. 4.5 shows bright clusters which are the TA signal, originally thought to be arising from the AmB molecules. These clusters are apparent after nearly 90 minutes of incubation and range from 0.5 - 1 mm in diameter. However, it is not apparent in these images where the yeast cells are relative to the clusters. The AmB did not, as expected, highlight the membrane of the fungal cells and make it clear how it was distributed among the plasma membrane as it appears to be internalized. This led to a need for additional measures to be taken to realize where the cells were located. Autofluorescent images were able to be acquired with the TAM images to identify the cell location and the AmB location simultaneously. Autofluorescence is the emission of fluorescence by naturally occurring biological structures located within the cells after absorption of light. We utilized our 400 nm pump which coincides with the naturally occurring absorption for many structures within the cells and monitored fluorescence at 470 nm using a photon counting photo multiplier tube. This signal was collected in the epi direction through a separate port on the microscope while the TA signal of AmB was still collected in the through direction as noted earlier. This allowed

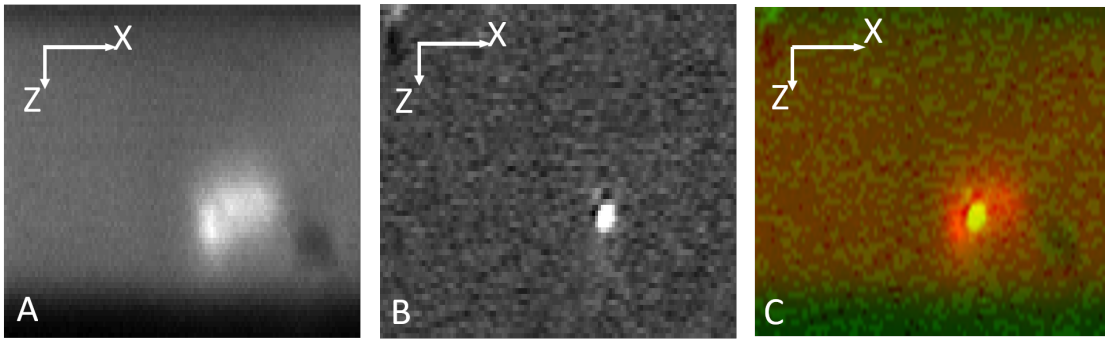

Figure 4.7: X-Z images of 250 μm AmB interacting with an *S. cerevisiae cell.* (A) Autofluorescence image locating the cell, (B) TAM image to locate the AmB appearing as a bright dot, (C) overlay of the two images to show where the AmB is located within the cell. All scale bars are 2 μm.

for both images to be acquired simultaneously. As seen in Fig. 4.6 the red signal is from autofluorescence detected at 470 nm while the green signal is TA arising from AmB detected at 550 nm. As an initial scan, it seems as though the AmB is being internalized into the cell in large clusters and not within the membrane. However, we do not yet have a full picture of where the AmB is sitting within the cell. This is only allowing us to see the two-dimensional picture in x and y, while we need the information in the z dimension to be sure that the AmB is indeed being internalized and not sitting on a top or bottom membrane of the cell.

Initial attempts were made to obtain a 3-D image of the AmB and yeast cells as seen in Fig. 4.7. Shown in A and B are the autofluorescence and TA signal respectively while C is the overlay image of A and B. As seen in Fig. 4.7 **A** the bottom of the flow cell in which a solution of YPD and AmB are flowing, the yeast cell is immobilized on the bottom coverslip. A higher background of fluorescence is then seen due to the fluorescence arising from the YPD media. This was an issue when attempting to achieve a higher signal to noise ratio for a sharper and more detailed image of the exact outline of the cell. The TA image looks similar to the previous images in the x/y dimensions with no signal present except where the AmB is located showing up as a bright cluster. The overlay of these two seems to show that the AmB is located internally near the top of the cell. Further attempts to acquire 3-D images of the AmB interacting with cells in alternative and less fluorescent media have been unsuccessful to this point.

Some attempts were also made at increasing the AmB concentration to identify if our limit of detection was simply too high to recognize AmB moving through the cell membranes. In Fig. 4.8 AmB at 250 μM was incubated with the yeast cells for 30 min in YPD. Both of these images were then acquired 30 and 40 min respectively after immobilization onto the coverslip. The red circles in the figure are highlighting where two yeast cells are located and the white signal is the TA signal of AmB. Both of these images were taken at an interpulse delay of 500 fs with a pixel dwell time of 10 ms and a total image acquisition time of approximately 3 min. As seen in Fig. 4.8a after 30 min the AmB is showing up near the membrane while ten minutes later in Fig. 4.8b the AmB signal is beginning to move further internal and away from the cell membrane in the bottom cell. These images suggest that it is necessary to have a higher AmB concentration in order to obtain images that are identifying the AmB before it becomes more concentrated in clusters.

For determination of the origination of the TA signal in the images, some controls were tested to ensure that the 'clusters' did not arise without the presence of AmB. This was done with all sample prep the same as described above with the exception of the addition of AmB. As seen in Fig. 4.9, there is a large TA signal arising from what appears to be similar clusters to the previous images. However, without the addition of AmB, it is not possible for this signal to be arising from AmB. Additionally, this signal is not arising solely from the same position as the yeast cells. It appears to be arising from the solution surrounding the cells. While in the previous images containing AmB clusters appeared after 30 - 90 minutes,

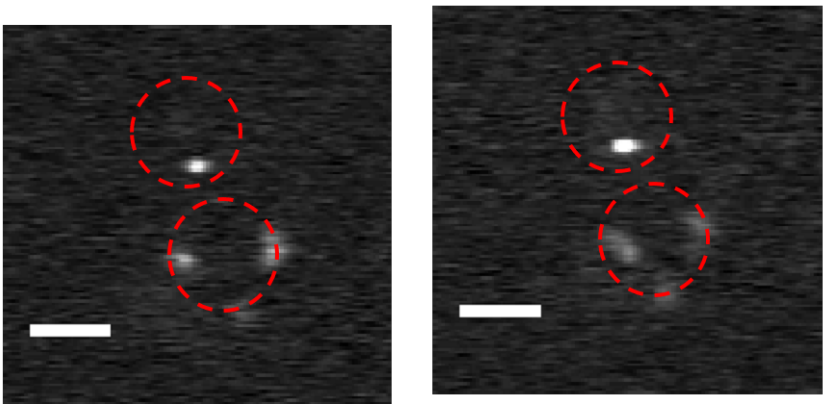

Figure 4.8: TAM of AmB in YPD at 250 μM taken 30 after AmB introduced. (b) taken immediately after (a) Scale bars are 2 μm.

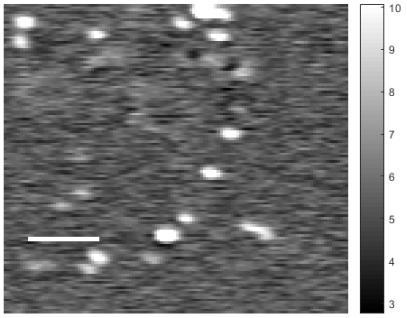

Figure 4.9: TAM image of a control sample of yeast containing no AmB. Scale bar is 2 μm.

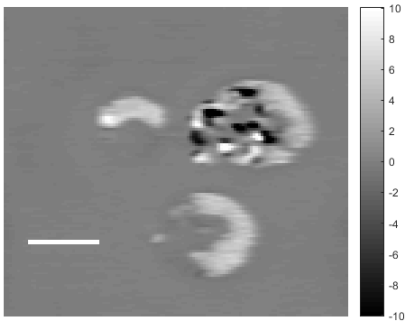

Figure 4.10: Additional TAM images of control samples of yeast cells with no AmB added before imaging. Scale bar is 2 μm.

the clusters shown in the control study appeared after over two hours of laser scanning. Later in the studies of AmB further investigation into the control samples were studied, and yielding different results. Fig. 4.10 is an image containing 3 yeast cells all showing TA signal appearing only to come from the same location as the cells. Once again these samples have not been exposed to AmB and therefore the TA signal can not be arising from AmB, but some other source either within the media or cells.

4.2.3 Future Directions

With the use of TAM we were able to successfully image what appears to be AmB, label free, interacting with living *S. cerevisiae* cells for the first time. While we realize that the control studies have shown inconsistencies, there are some indications that the control images

are arising from different sources than the images obtained with AmB present. The most convincing reason is the images shown in Fig. 4.8, where we have seen a concentration dependent time scale. With the addition of a higher concentration of AmB the signal began to arise quicker than previous studies and appeared as less concentrated clusters initially. Additionally, the clusters shown in the first control study appear to be arising from areas in the media where there are no yeast cells present, while the AmB images only have appeared co-localized with the yeast cells. The observation of internalized clusters does not match any of the three previously proposed mechanisms of action for AmB. Moving forward, we intend to image the AmB-cell interaction at different time intervals to characterize the internalization behavior. Future work with AmB and TAM imaging can take many different directions. Further investigations into acquiring accurate 3-D images should be of high importance to confirm the internalization of the drug. The 3-D imaging can also take place at specific time intervals at differing concentrations of AmB to allow for a full picture of the time and concentration dependence on the internalization of the drug. In order to get a clean image of AmB in 3-D the solvent in which the AmB is being delivered will have to be changed from YPD to a less fluorescent choice. This can be done in multiple ways with the use of clinically formulated AmB-lipid formulations or switched to a low-fluorescent media. Overall TAM has been shown to be a viable tool to utilize for the label-free imaging of AmB interacting with live cells and could be applied to multiple other small-molecule drug systems for imaging.

Chapter 5

Conclusions and Future Directions

We have been able to successfully construct a transient absorption microscope and demonstrate its imaging capabilities with a study of polystyrene beads and preliminary studies of AmB interacting with yeast cells. Unique to our setup, we have utilized the visible white light spectrum of a PCF fiber and demonstrated its abilities to be optimally compressed in a microscope. Upon exiting the fiber the white light contains a large amount of dispersion, leaving it with a pulse width beyond 1 ps. Through the use of a prism compression line and an SLM-based pulse shaper we have compressed this pulse to less than 100 fs. Once compressed, we were able to utilize the short pulses to image the beads and monitor the differences in excited state lifetimes of IR 1-44 in solution and at the surfaces of the beads.

After Initially constructing the instrument and characterizing the pulse widths, we were able to perform preliminary AmB studies. The current literature on the mechanism of action on AmB is varied and contains multiple conflicting results. We are utilizing TAM to directly image AmB interacting with live yeast cells for the first time. Preliminary images led us to believe that the AmB was being internalized in large clusters. When tested with a set of controls, however, the images still appeared to have clusters of signal arising with TAM. This has lead us to question our initial results, but we then imaged what appears to be a faster time dependence when tested with a higher concentration of AmB and clusters appearing near the membrane. This leaves us with a clear need for further TA studies of AmB interacting with live yeast cells. We hypothesize that the clusters which have appeared in the control studies may be arising from an interaction between the DMSO and YPD media. Future

studies will be performed using different formulations of AmB and/or yeast cells grown in a low-fluorescent media, which should result in a lower amount of background fluorescence and possibly un-reactive with DMSO. Overall, we have constructed and characterized a functioning transient absorption microscope and have shown TAM to be a plausible tool for effectively imaging AmB in a label-free manner.

Bibliography

[1] Amat-Roldán, I., Cormack, I. G., Loza-Alvarez, P., Gualda, E. J., and Artigas, D. (2004). Ultrashort pulse characterisation with shg collinear-frog. *Optics express*, 12(6):1169–1178. 11, 25

[2] Anderson, T. M., Clay, M. C., Cioffi, A. G., Diaz, K. A., Hisao, G. S., Tuttle, M. D., Nieuwkoop, A. J., Comellas, G., Maryum, N., Wang, S., et al. (2014). Amphotericin forms an extramembranous and fungicidal sterol sponge. *Nature chemical biology*, 10(5):400. 31

[3] Bakulin, A. A., Rao, A., Pavelyev, V. G., van Loosdrecht, P. H., Pshenichnikov, M. S., Niedzialek, D., Cornil, J., Beljonne, D., and Friend, R. H. (2012). The role of driving energy and delocalized states for charge separation in organic semiconductors. *Science*, 335(6074):1340–1344. 22

[4] Bates, D., Su, L., Yu, D., CHertow, G., Seger, D., Gomes, D., Dasbach, E., and Platt, R. (2001). Mortality and costs of acute renal failure associated with amphotericin b therapy. *Clinical Infectious Deisseases*, 32(5):686–693. 1

[5] Berera, R., van Grondelle, R., and Kennis, J. T. (2009). Ultrafast transient absorption spectroscopy: principles and application to photosynthetic systems. *Photosynthesis research*, 101(2-3):105–118. 22

[6] Billsten, H. H., Sundström, V., and Polívka, T. (2005). Self-assembled aggregates of the carotenoid zeaxanthin: time-resolved study of excited states. *The Journal of Physical Chemistry A*, 109(8):1521–1529. 33

[7] Bolard, J., Seigneuret, M., and Boudet, G. (1980). Interaction between phospholipid bilayer membranes and the polyene antibiotic amphotericin b: lipid state and cholesterol content dependence. *Biochimica et Biophysica Acta (BBA)-Biomembranes*, 599(1):280–293. 2

[8] Brixner, T. and Gerber, G. (2001). Femtosecond polarization pulse shaping. *Optics Letters*, 26(8):557–559. 28

[9] Brown, G. D., Denning, D. W., Gow, N. A., Levitz, S. M., Netea, M. G., and White, T. C. (2012). Hidden killers: human fungal infections. *Science translational medicine*, 4(165):165rv13–165rv13. 1

[10] Caffrey, P., Lynch, S., Flood, E., Finnan, S., and Oliynyk, M. (2001). Amphotericin biosynthesis in streptomyces nodosus: deductions from analysis of polyketide synthase and late genes. *Chemistry & biology*, 8(7):713–723. 30

[11] Calhoun, T. R., Davis, J. A., Graham, M. W., and Fleming, G. R. (2012). The separation of overlapping transitions in β-carotene with broadband 2d electronic spectroscopy. *Chemical Physics Letters*, 523:1–5. 24

[12] Carroll, E., Hill, M., Madsen, D., Malley, K., and Larsen, D. (2009). A single source femtosecond-millisecond broadband spectrometer. *Review of Scientific Instruments*, 80(2):026102. 23

[13] Chong, S., Min, W., and Xie, X. S. (2010). Ground-state depletion microscopy: detection sensitivity of single-molecule optical absorption at room temperature. *The Journal of Physical Chemistry Letters*, 1(23):3316–3322. 3

[14] Cifani, C., Costantino, S., Massi, M., et al. (2012). Commercially available lipid formulations of amphotericin b: are they bioequivalent and therapeutically equivalent? *Acta Bio Medica Atenei Parmensis*, 83(2):154–163. 30

[15] Curtin, A. E., Skinner, R., and Sanders, A. W. (2015). A simple metric for determining resolution in optical, ion, and electron microscope images. *Microscopy and Microanalysis*, 21(3):771–777. 27

[16] Davydova, D., de la Cadena, A., Akimov, D., and Dietzek, B. (2016). Transient absorption microscopy: Advances in chemical imaging of photoinduced dynamics. *Laser & Photonics Reviews*, 10(1):62–81. 22

[17] Dawlaty, J. M., Shivaraman, S., Chandrashekhar, M., Rana, F., and Spencer, M. G. (2008). Measurement of ultrafast carrier dynamics in epitaxial graphene. *Applied Physics Letters*, 92(4):042116. 22

[18] Denk, W., Strickler, J. H., and Webb, W. W. (1990). Two-photon laser scanning fluorescence microscopy. *Science*, 248(4951):73–76. 4

[19] Denk, W., Strickler, J. P., and Webb, W. W. (1991). Two-photon laser microscopy. US Patent 5,034,613. 4

[20] Diels, J.-C. and Rudolph, W. (2006). *Ultrashort laser pulse phenomena: fundamentals, techniques, and applications on a femtosecond time scale*. Elsevier. 6

[21] Dudley, J. M., Genty, G., and Coen, S. (2006). Supercontinuum generation in photonic crystal fiber. *Reviews of modern physics*, 78(4):1135. 23

[22] Ermishkin, L., Kasumov, K. M., and Potzeluyev, V. (1976). Single ionic channels induced in lipid bilayers by polyene antibiotics amphotericin b and nystatine. *Nature*, 262(5570):698. 31

[23] Fischer, M. C., Wilson, J. W., Robles, F. E., and Warren, W. S. (2016). Invited review article: pump-probe microscopy. *Review of Scientific Instruments*, 87(3):031101. 22

[24] Fu, D., Ye, T., Matthews, T. E., Chen, B. J., Yurtserver, G., and Warren, W. S. (2007). High-resolution in vivo imaging of blood vessels without labeling. *Optics letters*, 32(18):2641–2643. 3, 5, 22

[25] Genty, G., Lehtonen, M., and Ludvigsen, H. (2005). Route to broadband blue-light generation in microstructured fibers. *Optics letters*, 30(7):756–758. 24

[26] Gomez-Lopez, A., Buitrago, M. J., Rodriguez-Tudela, J. L., and Cuenca-Estrella, M. (2011). In vitro antifungal susceptibility pattern and ergosterol content in clinical yeast strains. *Revista iberoamericana de micologia*, 28(2):100–103. 2

[27] Grumstrup, E. M., Gabriel, M. M., Cating, E. E., Van Goethem, E. M., and Papanikolas, J. M. (2015). Pump–probe microscopy: Visualization and spectroscopy of ultrafast dynamics at the nanoscale. *Chemical Physics*, 458:30–40. 22

[28] Gruszecki, W. I., Luchowski, R., Gagoś, M., Arczewska, M., Sarkar, P., Hereć, M., Myśliwa-Kurdziel, B., Strzałka, K., Gryczynski, I., and Gryczynski, Z. (2009). Molecular

organization of antifungal antibiotic amphotericin b in lipid monolayers studied by means of fluorescence lifetime imaging microscopy. *Biophysical chemistry*, 143(1-2):95–101. 33

[29] Guo, Z., Manser, J. S., Wan, Y., Kamat, P. V., and Huang, L. (2015). Spatial and temporal imaging of long-range charge transport in perovskite thin films by ultrafast microscopy. *Nature communications*, 6:7471. 5, 22

[30] Hartung, A., Heidt, A. M., and Bartelt, H. (2011). Design of all-normal dispersion microstructured optical fibers for pulse-preserving supercontinuum generation. *Optics express*, 19(8):7742–7749. 25

[31] Heese-Peck, A., Pichler, H., Zanolari, B., Watanabe, R., Daum, G., and Riezman, H. (2002). Multiple functions of sterols in yeast endocytosis. *Molecular biology of the cell*, 13(8):2664–2680. 31

[32] Heidt, A. M., Hartung, A., Bosman, G. W., Krok, P., Rohwer, E. G., Schwoerer, H., and Bartelt, H. (2011). Coherent octave spanning near-infrared and visible supercontinuum generation in all-normal dispersion photonic crystal fibers. *Optics express*, 19(4):3775–3787. 23

[33] Hilligsøe, K. M., Andersen, T. V., Paulsen, H. N., Nielsen, C. K., Mølmer, K., Keiding, S., Kristiansen, R., Hansen, K. P., and Larsen, J. J. (2004). Supercontinuum generation in a photonic crystal fiber with two zero dispersion wavelengths. *Optics Express*, 12(6):1045–1054. 24, 25

[34] Jiang, X., Joly, N. Y., Finger, M. A., Babic, F., Wong, G. K., Travers, J. C., and Russell, P. S. J. (2015). Deep-ultraviolet to mid-infrared supercontinuum generated in solid-core zblan photonic crystal fibre. *Nature Photonics*, 9(2):133–139. 24

[35] Joo, T., Jia, Y., Yu, J.-Y., Lang, M. J., and Fleming, G. R. (1996). Third-order nonlinear time domain probes of solvation dynamics. *The Journal of chemical physics*, 104(16):6089–6108. 22

[36] Kamiński, D. M. (2014). Recent progress in the study of the interactions of amphotericin b with cholesterol and ergosterol in lipid environments. *European biophysics journal*, 43(10-11):453–467. 1, 32

[37] Kee, T. W. (2014). Femtosecond pump–push–probe and pump–dump–probe spectroscopy of conjugated polymers: New insight and opportunities. *The journal of physical chemistry letters*, 5(18):3231–3240. 28

[38] Kudlinski, A., George, A., Knight, J., Travers, J., Rulkov, A., Popov, S., and Taylor, J. (2006). Zero-dispersion wavelength decreasing photonic crystal fibers for ultraviolet-extended supercontinuum generation. *Optics Express*, 14(12):5715–5722. 24

[39] Léonard, J., Lecong, N., Likforman, J.-P., Crégut, O., Haacke, S., Viale, P., Leproux, P., and Couderc, V. (2007). Broadband ultrafast spectroscopy using a photonic crystal fiber: application to the photophysics of malachite green. *Optics express*, 15(24):16124–16129. 23

[40] Li, J., Zhang, W., Chung, T.-F., Slipchenko, M. N., Chen, Y. P., Cheng, J.-X., and Yang, C. (2015). Highly sensitive transient absorption imaging of graphene and graphene oxide in living cells and circulating blood. *Scientific reports*, 5:12394. 22

[41] Linden, S., Giessen, H., and Kuhl, J. (1998). Xfroga new method for amplitude and phase characterization of weak ultrashort pulses. *physica status solidi (b)*, 206(1):119–124. 12, 25

[42] Link, S. and El-Sayed, M. A. (2003). Optical properties and ultrafast dynamics of metallic nanocrystals. *Annual review of physical chemistry*, 54(1):331–366. 22

[43] Liu, J. and Irudayaraj, J. M. (2016). Non-fluorescent quantification of single mrna with transient absorption microscopy. *Nanoscale*, 8(46):19242–19248. 22

[44] Lopez-Berestein, G., Mehta, R., Hopfer, R., Mehta, K., Hersh, E., and Juliano, R. (1983). Effects of sterols on the therapeutic efficacy of liposomal amphotericin b in murine candidiasis. *Cancer Drug Delivery*, 1(1):37–42. 30

[45] Massaro, E. S., Hill, A. H., and Grumstrup, E. M. (2016). Super-resolution structured pump–probe microscopy. *ACS Photonics*, 3(4):501–506. 23

[46] McNamara, C., Crawforth, J., Hickman, B., Norwood, T., Rawlings, B., et al. (1998). Biosynthesis of amphotericin b. *Journal of the Chemical Society, Perkin Transactions 1*, (1):83–88. 30

[47] Medoff, G., Brajtburg, J., Kobayashi, G., and Bolard, J. (1983). Antifungal agents useful in therapy of systemic fungal infections. *Annual review of pharmacology and toxicology*, 23(1):303–330. 1

[48] Min, W., Freudiger, C. W., Lu, S., and Xie, X. S. (2011). Coherent nonlinear optical imaging: beyond fluorescence microscopy. *Annual review of physical chemistry*, 62:507–530. 22

[49] Min, W., Lu, S., Chong, S., Roy, R., Holtom, G. R., and Xie, X. S. (2009). Imaging chromophores with undetectable fluorescence by stimulated emission microscopy. *Nature*, 461(7267):1105. 3, 22

[50] Mohanty, J., Palit, D., and Mittal, J. (2000). Photophysical properties of two infrared laser dyes–ir-144 and ir-140: A picosecond laser flash photolysis study. *Proceedings-Indian National Science Academy Part A*, 66(2):303–315. 26

[51] Monk, B. C. and Goffeau, A. (2008). Outwitting multidrug resistance to antifungals. *Science*, 321(5887):367–369. 1, 30

[52] Ostroumova, O. S., Efimova, S. S., and Schagina, L. V. (2012). Probing amphotericin b single channel activity by membrane dipole modifiers. *PLoS One*, 7(1):30261. 2

[53] Parks, L. W. (1995). Regulation and functions of sterols in yeast. In *Plant Lipid Metabolism*, pages 347–349. Springer. 31

[54] Robles, A., Fischer, M., and Warren, W. (2014). Femtosecond pulse shaping enables detection of optical kerr-effect (oke) dynamics for molecular imaging. *Optics Letters*, 39:4788–4791. 28

[55] Rodriguez, R. J., Low, C., Bottema, C. D., and Parks, L. W. (1985). Multiple functions for sterols in saccharomyces cerevisiae. *Biochimica et Biophysica Acta (BBA)-Lipids and Lipid Metabolism*, 837(3):336–343. 31

[56] Rullière, C., Amand, T., and Marie, X. (1998). Spectroscopic methods for analysis of sample dynamics. In *Femtosecond laser pulses*, pages 203–259. Springer. 6

[57] Sangalli-Leite, F., Scorzoni, L., Mesa-Arango, A. C., Casas, C., Herrero, E., Gianinni, M. J. S. M., Rodríguez-Tudela, J. L., Cuenca-Estrella, M., and Zaragoza, O. (2011). Amphotericin b mediates killing in cryptococcus neoformans through the induction of a strong oxidative burst. *Microbes and infection*, 13(5):457–467. 32

[58] Schnedermann, C., Lim, J. M., Wende, T., Duarte, A. S., Ni, L., Gu, Q., Sadhanala, A., Rao, A., and Kukura, P. (2016). Sub-10 fs time-resolved vibronic optical microscopy. *The journal of physical chemistry letters*, 7(23):4854–4859. 22

[59] Shang, X., Benderskii, A. V., and Eisenthal, K. B. (2001). Ultrafast solvation dynamics at silica/liquid interfaces probed by time-resolved second harmonic generation. *The Journal of Physical Chemistry B*, 105(47):11578–11585. 26

[60] Simpson, M. J., Doughty, B., Yang, B., Xiao, K., and Ma, Y.-Z. (2015). Spatial localization of excitons and charge carriers in hybrid perovskite thin films. *The journal of physical chemistry letters*, 6(15):3041–3047. 5, 22

[61] Sokol-Anderson, M. L., Brajtburg, J., and Medoff, G. (1986). Amphotericin b-induced oxidative damage and killing of candida albicans. *Journal of Infectious Diseases*, 154(1):76–83. 31, 32

[62] Tobudic, S., Kratzer, C., and Presterl, E. (2012). Azole-resistant candida spp.–emerging pathogens? *Mycoses*, 55:24–32. 1, 30

[63] Tong, L., Liu, Y., Dolash, B. D., Jung, Y., Slipchenko, M. N., Bergstrom, D. E., and Cheng, J.-X. (2012). Label-free imaging of semiconducting and metallic carbon nanotubes in cells and mice using transient absorption microscopy. *Nature nanotechnology*, 7(1):56. 22

[64] Trebino, R. (2012). *Frequency-resolved optical gating: the measurement of ultrashort laser pulses*. Springer Science & Business Media. 11, 25

[65] Trebino, R., DeLong, K. W., Fittinghoff, D. N., Sweetser, J. N., Krumbügel, M. A., Richman, B. A., and Kane, D. J. (1997). Measuring ultrashort laser pulses in the time-frequency domain using frequency-resolved optical gating. *Review of Scientific Instruments*, 68(9):3277–3295. 11

[66] Tu, H., Liu, Y., Turchinovich, D., and Boppart, S. A. (2011). Compression of fiber supercontinuum pulses to the fourier-limit in a high-numerical-aperture focus. *Optics letters*, 36(12):2315–2317. 23

[67] Vaughan, J. C., Hornung, T., Feurer, T., and Nelson, K. A. (2005). Diffraction-based femtosecond pulse shaping with a two-dimensional spatial light modulator. *Optics letters*, 30(3):323–325. 24

[68] Villafana, T. E., Brown, W. P., Delaney, J. K., Palmer, M., Warren, W. S., and Fischer, M. C. (2014). Femtosecond pump-probe microscopy generates virtual cross-sections in historic artwork. *Proceedings of the National Academy of Sciences*, 111(5):1708–1713. 5, 22

[69] Vincent, B. M., Lancaster, A. K., Scherz-Shouval, R., Whitesell, L., and Lindquist, S. (2013). Fitness trade-offs restrict the evolution of resistance to amphotericin b. *PLoS biology*, 11(10):e1001692. 2

[70] von Vacano, B., Wohlleben, W., and Motzkus, M. (2006). Actively shaped supercontinuum from a photonic crystal fiber for nonlinear coherent microspectroscopy. *Optics letters*, 31(3):413–415. 23

[71] Weiner, A. M. (2000). Femtosecond pulse shaping using spatial light modulators. *Review of scientific instruments*, 71(5):1929–1960. 24

Vita

Kevin Higgins was born on March 1, 1991 in Nampa, Idaho to Jeff and Melanie Higgins. He was raised in the nearby town of Kuna, Idaho where he graduated from high school at Kuna High in 2009. Kevin then attended Idaho State University where he studied chemistry. While at ISU Kevin performed undergraduate research under the guidance of Dr. John Kalivas where they performed chemometric research. He obtained a Bachelors of Arts degree from Idaho State University in 2013. Kevin then chose to move to Knoxville, Tennessee where he would pursue a graduate degree from the University of Tennessee, Knoxville in analytical chemistry under the guidance of Dr. Tessa Calhoun.